Interaction of Waves with Frictional Interfaces Using Summation-by-Parts Difference Operators: Weak Enforcement of Nonlinear Boundary Conditions

Jeremy E. Kozdon · Eric M. Dunham · Jan Nordström

Abstract We present a high-order difference method for problems in elastodynamics involving the interaction of waves with highly nonlinear frictional interfaces. We restrict our attention to two-dimensional antiplane problems involving deformation in only one direction. Jump conditions that relate tractions on the interface, or fault, to the relative sliding velocity across it are of a form closely related to those used in earthquake rupture models and other frictional sliding problems. By using summation-by-parts (SBP) finite difference operators and weak enforcement of boundary and interface conditions, a strictly stable method is developed. Furthermore, it is shown that unless the nonlinear interface conditions are formulated in terms of characteristic variables, as opposed to the physical variables in terms of which they are more naturally stated, the semi-discretized system of equations can become extremely stiff, preventing efficient solution using explicit time integrators.

The use of SBP operators also provides a rigorously defined energy balance for the discretized problem that, as the mesh is refined, approaches the exact energy balance in the continuous problem. This enables one to investigate earthquake energetics, for example the efficiency with which elastic strain energy released during rupture is converted to radiated energy carried by seismic waves, rather than dissipated by frictional sliding of the fault. These theoretical results are confirmed by several numerical tests in both one and two dimensions demonstrating the computational efficiency, the high-order convergence rate of the method, the benefits of using strictly stable numerical methods for long time integration, and the accuracy of the energy balance.

Keywords High order finite difference · Nonlinear boundary conditions · Simultaneous approximation term method · Elastodynamics · Summation-by-parts · Friction · Wave propagation

J.E. Kozdon (✉) · E.M. Dunham
Department of Geophysics, Stanford University, Stanford, CA 94305, USA
e-mail: jkozdon@stanford.edu

J. Nordström
Department of Mathematics, Linköping University, 581 83, Linköping, Sweden

1 Introduction

Problems involving frictional contacts between solids are important in many fields including earthquake dynamics, fracture mechanics, and structural engineering and design. For many of these problems the material can be modeled as linear elastic with frictional sliding occurring on infinitesimally thin internal interfaces, or faults, governed by nonlinear friction laws. As relative motion occurs across the interface (with the discontinuity in tangential displacement referred to as slip) nonlinear relations relate the slip velocity to the tractions acting on the fault.

In order to match the frictional behavior seen in experiments, the friction laws used in practice must depend not only on slip velocity and tractions acting on the fault but also, for example, on the history of sliding, frictional heat generation, and other process occurring within the fault zone. Friction laws with this more complex structure are referred to as rate-and-state friction laws. In this work we assume that the fault shear strength τ (resistance to slip) depends only on the slip velocity V through the friction law $\tau = F(V)$. Furthermore, we consider only antiplane loading with deformation in only one direction; hence the equations of elasticity simplify to three partial differential equations (PDEs) for one component of velocity and two components of stress.

Our primary motivation is the need for provably stable, accurate, and efficient methods for modeling earthquake rupture propagation on faults governed by velocity-dependent friction laws. Spontaneous rupture models are becoming increasingly used to study scenario earthquakes and to assess seismic hazard. In addition to providing predictions of ground shaking, these models can also be employed to investigate fundamental questions of earthquake energetics. The elastic strain energy liberated during an earthquake by fault slip and stress relaxation is partitioned between energy dissipated during frictional sliding and the energy carried by radiated waves into the far-field. Radiated seismic energy is one of a very limited set of observable global earthquake source parameters, and, together with estimates of the change in strain energy from measurements of rupture area and total slip, can be used to estimate the energy dissipated on the fault. This technique places valuable constraints on the frictional properties of faults at depth.

In this work, we use summation-by-parts (SBP) finite difference methods [3, 12, 13, 16, 28] on an unstaggered grid. The advantage of these methods is that after appropriate boundary treatment the numerical methods can be proven to mimic the energy dissipation properties of the continuous problem, leading to what is known as strict stability [8] (see Sect. 3); strictly stable methods are important for long time integration as the solution is not degraded by small scale error growth. SBP methods come equipped with a rigorously defined numerical energy balance that, with mesh refinement, converges to the exact energy balance of the continuous problem. We demonstrate in this work how the method can be used to accurately calculate various contributions to the global energy balance (i.e., the work done on the elastic body by boundary tractions, the energy dissipated on the fault, and the change in mechanical energy of the elastic body).

A field, $v(y)$, is discretized on a uniform grid spanning the unit interval:

$$v_i = v(y_i), \quad y_i = ih, \quad i = 0, \dots, N, \tag{1}$$

where $h = 1/N$ is the grid spacing and y_0 and y_N are on the left and right boundaries, respectively. A difference approximation to the first derivative is said to be of SBP form if it can be written as

$$\frac{\partial v}{\partial y} \approx \boldsymbol{H}^{-1} \boldsymbol{Q} \, \boldsymbol{v}, \tag{2}$$

where $\boldsymbol{H}$ is a symmetric positive definite matrix, $\boldsymbol{Q}$ is an almost skew-symmetric matrix with $\boldsymbol{Q}^T + \boldsymbol{Q} = \textbf{diag}[-1\ 0\ \cdots\ 0\ 1]$, and the vector $\boldsymbol{v} = (v_0, v_1, \ldots, v_N)^T$ is the grid data. For instance, the second order SBP operator is [12]

$$\boldsymbol{H} = h\, \textbf{diag} \left[\tfrac{1}{2}\ 1\ 1\ \cdots\ 1\ \tfrac{1}{2} \right], \quad \boldsymbol{Q} = \frac{1}{2} \begin{bmatrix} -1 & 1 & & & \\ -1 & 0 & 1 & & \\ & \ddots & \ddots & \ddots & \\ & & -1 & 0 & 1 \\ & & & -1 & 1 \end{bmatrix}. \tag{3}$$

Defining the continuous and discrete inner products,

$$(u, v) = \int_0^1 u(y)v(y)\, dy \quad \text{and} \quad (\boldsymbol{u}, \boldsymbol{v})_h = \boldsymbol{u}^T \boldsymbol{H} \boldsymbol{v}, \tag{4}$$

it becomes clear why these methods are called SBP methods as they mimic the integration-by-parts property of the continuous problem,

$$\left(v, \frac{dv}{dy} \right) = \int_0^1 v\, \frac{dv}{dy}\, dy = \frac{1}{2} \left[v(1)^2 - v(0)^2 \right], \tag{5}$$

$$(\boldsymbol{v}, \boldsymbol{H}^{-1} \boldsymbol{Q} \boldsymbol{v})_h = \boldsymbol{v}^T\ \boldsymbol{Q}\ \boldsymbol{v} = \frac{1}{2} \boldsymbol{v}^T\ (\boldsymbol{Q} + \boldsymbol{Q}^T)\ \boldsymbol{v} = \frac{1}{2}(v_N^2 - v_0^2). \tag{6}$$

SBP operators are constructed from central difference methods, with orders $q = 2, 4, 6, 8, \ldots$ in the interior, and transition near boundaries to one-sided difference methods in a manner that maintains the SBP property. Generally, the transition to one-sided near the boundary lowers the local accuracy of the method to r; hence, the global accuracy of the method is $p = r + 1$ [7, 29]. There are two classes of SBP operators: diagonal norm (diagonal $\boldsymbol{H}$) and block norm operators (non-diagonal $\boldsymbol{H}$). The diagonal norm operators have interior accuracy $q = 2s$ ($s = 1, 2, \ldots$) and boundary accuracy $r = s$, so the global accuracy is $p = s + 1$, whereas block norm operators can have boundary accuracy $r = 2s - 1$ and thus global accuracy $p = 2s$. There are drawbacks to using the block norm operators, the most prominent being difficulties in proving stability for problems which involve variable coefficients and/or coordinate transforms [18, 20, 24, 30]. In this work we exclusively consider the diagonal norm operators and methods are referred to by their global accuracy.

By using SBP methods, along with suitable boundary treatment, it is possible to design difference schemes that mimic the energy dissipation properties of the continuous PDE, resulting in a provably strictly stable discretization. There are numerous methods for incorporating boundary conditions; the two considered in this work are the injection method, which enforces boundary conditions strongly, and the simultaneous approximation term (SAT) method [2], which enforces boundary conditions weakly. In the injection method the grid values at the boundary points are modified so that they strictly satisfy the boundary conditions. Though this is conceptually straightforward, the method destroys the SBP property of the operator and stability can be difficult or impossible to prove [8]. Additionally, with the injection method corners of the computational domain in two dimensions (and edges in three dimensions) require special handling, and it is often unclear how to treat incompatible boundary conditions. With SAT the grid values are not directly modified, but a penalty term is added to the semi-discrete equations so that the difference operator is penalized for not satisfying the boundary conditions. With a carefully chosen penalty parameter, stability and accuracy are guaranteed.

As will be seen in Sect. 2, this work considers the equations of elasticity written in first-order form. This allows us to leverage the well established SBP-SAT technology for the first-order hyperbolic equations, including the use of coordinate transforms [20] and hybrid structured-unstructured methods [22]. Mattsson et al. [17] recently extended the SBP-SAT framework to the second-order wave equation, which reduces the number of unknowns and typically results in more efficient time-stepping and better dispersion properties. One of the complications with using the second-order equations is that the use of coordinate transforms introduces mixed derivatives. Additionally, plastic deformation is easily handled with source terms on the first-order equations, but time-stepping becomes much more difficult with the second-order form of the equations [5].

The remainder of this paper is as follows: In Sect. 2 well-posedness and the energy dissipation rate for the continuous problem are established. The discrete method is then discussed in Sect. 3 along with three procedures for including boundary conditions: the injection method and two formulations of the SAT method. The SAT procedure leads to numerical methods which dissipate energy at least as fast as the continuous solution (with the difference in the rates vanishing as the mesh is refined), thus ensuring strict stability. The computational benefits and drawbacks of the two SAT formulations are discussed in Sect. 4 and in Sect. 5 computational results demonstrate the theoretical results. Conclusions are presented in Sect. 6.

2 Continuous Problem: Well-Posedness and Energy Dissipation

Consider a homogeneous 2-D elastic medium with a frictional interface (or fault) located at $y = 0$ (Fig. 1a); for simplicity we assume that the domain is rectangular with lower left corner $(x, y) = (-L_x, -L_y)$ and upper right corner $(x, y) = (L_x, L_y)$. As indicated in the figure, superscript (1) is used throughout to denote variables in the region $y > 0$ and (2) is used to denote $y < 0$.

Considering only antiplane deformation, the governing equations in the elastic medium (momentum conservation and the time derivative of Hooke's law) can be written as

$$\rho \frac{\partial v_z}{\partial t} = \frac{\partial \sigma_{xz}}{\partial x} + \frac{\partial \sigma_{yz}}{\partial y}, \qquad \frac{\partial \sigma_{xz}}{\partial t} = G \frac{\partial v_z}{\partial x}, \qquad \frac{\partial \sigma_{yz}}{\partial t} = G \frac{\partial v_z}{\partial y}, \tag{7}$$

where v_z is the particle velocity in the z-direction (out of the page), σ_{xz} and σ_{yz} are components of shear stress which induce tractions (force per unit area) in the direction of the particle velocity on planes with unit normals $\hat{x}$ and $\hat{y}$, respectively, ρ is density, and G is shear modulus. With a change of variables the governing equations (7) can be written as a symmetric first order hyperbolic system:

$$\frac{\partial \boldsymbol{q}}{\partial t} = \begin{bmatrix} 0 & c_s & 0 \\ c_s & 0 & 0 \\ 0 & 0 & 0 \end{bmatrix} \frac{\partial \boldsymbol{q}}{\partial x} + \begin{bmatrix} 0 & 0 & c_s \\ 0 & 0 & 0 \\ c_s & 0 & 0 \end{bmatrix} \frac{\partial \boldsymbol{q}}{\partial y} = A_x \frac{\partial \boldsymbol{q}}{\partial x} + A_y \frac{\partial \boldsymbol{q}}{\partial y}, \tag{8}$$

$$\boldsymbol{q} = \begin{bmatrix} \sqrt{\frac{\rho}{2}} v_z & \frac{1}{\sqrt{2G}} \sigma_{xz} & \frac{1}{\sqrt{2G}} \sigma_{yz} \end{bmatrix}^T, \tag{9}$$

where $c_s = \sqrt{G/\rho}$ is the shear wave speed.

To fully specify the problem, boundary and interface conditions are needed. In order to determine the number of boundary conditions required, the characteristic form of the problem is considered; the number of boundary and interface conditions is equal to the
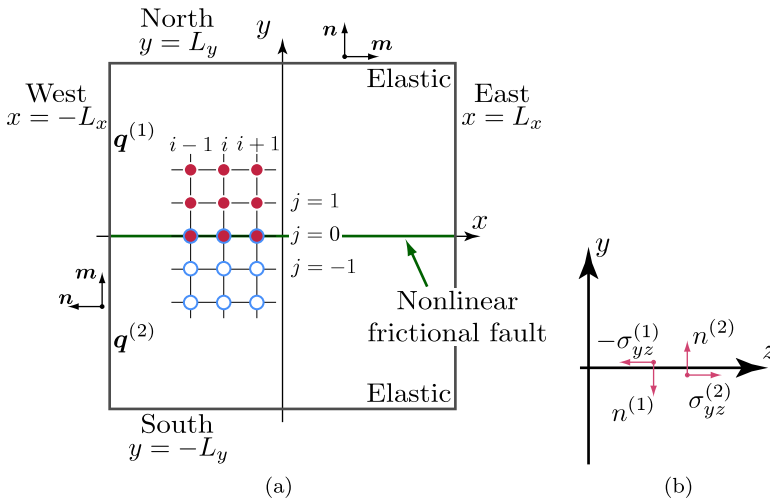
Fig. 1 (**a**) Problem domain consisting of two elastic bodies in contact along a nonlinear frictional fault at $y = 0$. The computational grid is unstaggered, i.e., velocity and stresses are collocated. $q^{(1)}$ and $q^{(2)}$ are the solutions for $y > 0$ and $y < 0$, respectively. Along the fault each grid node has two solutions, $q_{i0}^{(1)}$ and $q_{i0}^{(2)}$, in order to handle discontinuities in fields across the fault. At the boundaries and fault the unit normal n is defined to point outward, e.g., at the fault the unit normals are $n^{(1)} = -\hat{y}$ and $n^{(2)} = \hat{y}$, and $m = [n_y\ -n_x]^T$ is orthogonal to n. North, south, east, and west are used throughout to refer to the faces of the exterior domain. (**b**) Sideview illustrating tractions and sign convention for unit normal vectors. Fault normal direction to side (l) of the fault, $n^{(l)}$, points from side (l) to the other side. The shear traction (frictional force per unit surface area of the interface) exerted in the z-direction on side (l) of fault by the material on the other side is $n_i^{(l)}\sigma_{iz}$

number of characteristics propagating into the domain and out of the fault [11]. Since A_x and A_y in (8) are not simultaneously diagonalizable, we must consider the characteristic form in one direction only. Namely, the characteristic variables associated with waves propagating in the direction of the unit vector n are the eigenvectors of the system $n_i A_i$:

$$w^{\pm} = \sigma_{iz} n_i \mp Z v_z, \quad \text{with speeds } \pm c_s, \tag{10}$$

$$\mathring{w} = \sigma_{iz} m_i, \quad\quad\quad \text{with zero speed,} \tag{11}$$

$$m = [n_y\ -n_x]^T, \tag{12}$$

where $Z = \rho c_s = G/c_s$ is the shear impedance, summation over x, y is implied by repeated indices, n_i refers to the components of n, and m is orthogonal to n (chosen so that $n \times m = \hat{z}$). As indicated in Fig. 1a, at the exterior boundaries n is taken to be the outward pointing normal. With this convention the outward propagating characteristic variable is always w^+ and the incoming characteristic variable is always w^-. Thus, one boundary condition is needed on w^- at each boundary; we take these external boundary conditions to be linear functions of the form

$$w^- = R w^+, \tag{13}$$

where R is the reflection coefficient and can vary spatially along the boundary; in general, boundary condition (13) could also depend on the zero speed characteristic variable $\mathring{w}$. The boundary conditions can also be generalized to include a boundary data function $g(t)$. At

the exterior boundaries, as well as the fault, no special handling of the zero speed characteristic variable is needed for either the continuous or discrete problem [19, 21]. Several common boundary conditions can be expressed in this manner: $R = 0$, which is the non-reflecting boundary condition; $R = -1$, which is the traction free surface boundary condition ($\sigma_{iz} n_i = 0$); and $R = 1$, which is the rigid wall boundary condition ($v_z = 0$). There has been much work on the development of more effective non-reflecting boundary conditions, e.g., Hagstrom et al. [9] and Appelo et al. [1], but only the simple form outlined above is considered in this work as our primary interest is the treatment of the nonlinear frictional interface.

The fault is governed by a nonlinear interface relationship. Across the fault some of the fields (in particular the particle velocity) can be discontinuous, thus the characteristic variables (10) need not be continuous across the fault. Hence, characteristic variables propagating out of the fault into side (l) of the domain, $w^{-(l)}$, are related to the characteristic variables propagating into the fault from side (l) of the domain, $w^{+(l)}$, through a nonlinear relation of the form

$$w^{-(l)} = \mathcal{W}^{-(l)}\big(w^{+(1)}, w^{+(2)}\big), \tag{14}$$

where $\mathcal{W}^{-(l)}$ is a nonlinear function that, in general, is different for each side of the fault; more generally, $\mathcal{W}^{-(l)}$ could also depend on $\mathring{w}^{(l)}$ but this is not needed for the problems considered below. For example, if the interface was welded, meaning that the fields were continuous across the interface, they would take the form

$$w^{-(1)} = -w^{+(2)} \quad \text{and} \quad w^{-(2)} = -w^{+(1)}, \tag{15}$$

where the minus sign is due to the change in definition of outward pointing normal on either side of the fault.

In elastodynamics it is more common for the interface conditions (14) to be formulated in terms of the physical variables (velocity and stress) through a nonlinear friction law. We define the slip velocity $V(x, t) = v_z^{(1)}(x, 0, t) - v_z^{(2)}(x, 0, t)$ as the discontinuity in particle velocity across the fault (see Fig. 2). The shear traction exerted on side (l) of the fault by the material on the opposite side is $\sigma_{iz}^{(l)} n_i^{(l)}$ (see Fig. 1b). Force balance [6] requires that the tractions on opposite sides of the fault be equal in magnitude and opposite in sign. It follows that, for the specific case of a planar fault at $y = 0$ (see Fig. 2),

$$\sigma_{yz}^{(1)}(x, 0, t) = \sigma_{yz}^{(2)}(x, 0, t). \tag{16}$$

No such restriction exists for σ_{xz}, and for spatially nonuniform slip, σ_{xz} will be discontinuous across the fault (see Fig. 2).

We consider frictional faults on which the shear stress, defined as the traction on side (2) from side (1), is always equal to the shear strength (the frictional resistance to sliding): $\sigma_{iz}^{(l)} n_i^{(2)} = \tau(x, t)$, or, for the planar fault $y = 0$, $\sigma_{yz}^{(l)}(x, 0, t) = \tau(x, t)$. In this work we consider purely velocity dependent nonlinear friction laws:

$$\tau = F(V). \tag{17}$$

Many realistic friction laws introduce a set of state variables to F that evolve according to differential evolution equations.

The first theoretical result of this paper relates the characteristic form of the fault conditions (14) to the continuity condition (16) and the friction law (17):
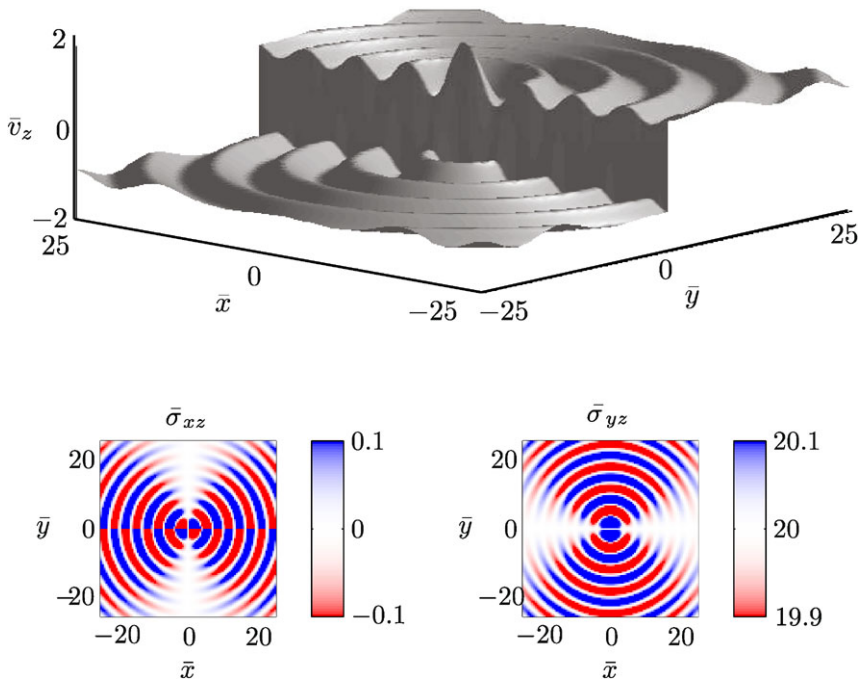
Fig. 2 Example of a 2-D solution, illustrating that v_z and σ_{xz} are discontinuous across the fault, whereas σ_{yz} is continuous. The specific solution shown is used as a verification problem (see Sect. 5 for details). In the plots for the stresses the color scale is saturated to show the detail of the solution. Velocity is shown at time $t = 2n\pi$ and stresses at time $t = (2n + 1)\pi/2$ for integer n

Proposition 1 *The interface conditions* (16) *and* (17) *(written in terms of the physical variables) can be uniquely expressed in the form of* (14) *(written in terms of the characteristic variables) if* $F'(V) \neq -Z/2$.

Proof Without loss of generality we prove the theorem for the case of a planar fault at $y = 0$ (see Fig. 1a), but the proposition holds for faults of arbitrary shape and orientation.

We first rewrite $\sigma_{yz}^{(l)}$ and the slip velocity V using the characteristic variables (10) and characteristic interface conditions (14):

$$\sigma_{yz}^{(1)} = -\frac{1}{2}\big(w^{+(1)} + \mathcal{W}^{-(1)}\big), \qquad \sigma_{yz}^{(2)} = \frac{1}{2}\big(w^{+(2)} + \mathcal{W}^{-(2)}\big), \tag{18}$$

$$V = \frac{1}{2Z}\big(\mathcal{W}^{-(1)} - w^{+(1)} - \mathcal{W}^{-(2)} - w^{+(2)}\big). \tag{19}$$

For example, if the welded interface condition of (15) is used, then (18) and (19) imply $\sigma_{yz}^{(1)} = \sigma_{yz}^{(2)}$ and $V = 0$ (or $v_z^{(1)} = v_z^{(2)}$), as expected.

Now, using (18) and (19) we rewrite the friction law (17) along with continuity of traction components of stress (16) as a nonlinear system:

$$\mathbf{0} = \begin{bmatrix} \sigma_{yz}^{(1)} - \sigma_{yz}^{(2)} \\ \sigma_{yz}^{(2)} - F(V) \end{bmatrix}. \tag{20}$$

The Jacobian determinant of (20) with respect to the variables $\mathcal{W}^{-(1)}$ and $\mathcal{W}^{-(2)}$ is

$$J = \det \begin{bmatrix} -\frac{1}{2} & -\frac{1}{2} \\ -\frac{1}{2Z}F'(V) & \frac{1}{2} + \frac{1}{2Z}F'(V) \end{bmatrix} = -\frac{1}{4Z}\left[Z + 2F'(V)\right]. \tag{21}$$

Since $J \neq 0$ if $F'(V) \neq -Z/2$, the proposition follows by the implicit function theorem. $\square$

For the problem to be well-posed a unique solution must exist, depending continuously on the boundary and initial data of the problem, and we must have an energy estimate [8]. A suitable energy estimate for our problem, where we have no boundary data or forcing functions (i.e., all external boundary conditions are homogeneous, and there are no source terms in the PDEs that would appear as nonzero body forces in the momentum equation and nonzero plastic strain rates in Hooke's law), is

$$\|\boldsymbol{q}(\cdot, t)\| \leq K_c e^{\alpha_c t} \|\boldsymbol{q}(\cdot, 0)\|, \tag{22}$$

where K_c and α_c are constants independent of the solution. In this work, the norm is taken to be the mechanical energy per unit distance in the z-direction in the solution,

$$\|\boldsymbol{q}(\cdot, \cdot, t)\|^2 = \iint_\Omega \boldsymbol{q}^T \boldsymbol{q} \, dx \, dy = \iint_\Omega \left(\frac{\rho}{2}v_z^2 + \frac{1}{2G}\sigma_{iz}\sigma_{iz}\right) dx \, dy, \tag{23}$$

where Ω is the problem domain. The first term is the kinetic energy and the second the elastic strain energy. If it can be shown that energy is dissipated, i.e.,

$$\frac{d\|\boldsymbol{q}\|^2}{dt} \leq 0, \tag{24}$$

then by integration (22) holds with $\alpha_c = 0$ and $K_c = 1$. For problem (8) we have

$$\begin{aligned} \frac{d\|\boldsymbol{q}\|^2}{dt} &= 2\iint_\Omega \boldsymbol{q}^T \frac{\partial \boldsymbol{q}}{\partial t} \, dx \, dy = 2\iint_\Omega \boldsymbol{q}^T \left(A_x \frac{\partial \boldsymbol{q}}{\partial x} + A_y \frac{\partial \boldsymbol{q}}{\partial y}\right) dx \, dy \\ &= \int_{\partial\Omega} v_z \sigma_{iz} n_i \, ds + \int_{-L_x}^{L_x} [v_z \sigma_{iz} n_i]_{y=0^+}^{0^-} \, dx \\ &= \int_{\partial\Omega} v_z \sigma_{iz} n_i \, ds - \int_{-L_x}^{L_x} V\tau \, dx, \end{aligned} \tag{25}$$

where $\partial\Omega$ is the domain boundary and we have used the divergence theorem to change area integrals to line integrals along the boundaries and fault. The first term in (25) represents the energy flux across the exterior boundaries [14] and the last term is the rate at which mechanical energy flows into the fault (where it is converted to heat during frictional sliding). It is straightforward to show that the exterior boundary terms are negative semi-definite with boundary condition (13) if $-1 \leq R \leq 1$, namely,

$$v_z \sigma_{iz} n_i = -\frac{1}{4Z}\left(1 - R^2\right)\left(w^+\right)^2 \leq 0. \tag{26}$$

If the friction law function $F(V)$ in (17) takes the sign of its argument or zero, then the last term in (25) associated with the fault is also negative semi-definite. Thus (25) is negative semi-definite and we have an energy estimate.

For linear problems with linear boundary conditions, energy dissipation implies uniqueness and, assuming existence, well-posedness [8]. For problems with nonlinear boundary conditions, energy dissipation only does not imply uniqueness due to the fact that the difference of two solutions does not satisfy the same boundary conditions as the original problem. Here we derive one further condition on F that ensures uniqueness of the solution.

Assume that $\boldsymbol{q}_1$ and $\boldsymbol{q}_2$ are solutions to (8) with boundary condition (13), interface conditions (16) and (17), and the same initial data; then $\boldsymbol{\Delta} = \boldsymbol{q}_1 - \boldsymbol{q}_2$ satisfies (8) with boundary conditions (13) and the modified interface conditions

$$\tau_1 - \tau_2 = F(V_1) - F(V_2) \quad \text{and} \quad \Delta\sigma_{yz}^{(1)} = \Delta\sigma_{yz}^{(2)}. \tag{27}$$

The energy dissipation rate of this problem is

$$\frac{d\|\boldsymbol{\Delta}\|^2}{dt} = \int_{\partial\Omega} \Delta v_z \Delta\sigma_{iz} n_i \, ds - \int_{-L_x}^{L_x} \Delta V \Delta\tau \, dx, \tag{28}$$

where the exterior boundary terms are negative semi-definite due the energy estimate and linearity of the exterior boundary conditions. The last term can be rewritten using the intermediate value theorem for some $V \in [V_1, V_2]$ as

$$\Delta V \, \Delta\tau = \Delta V \left[F(V_1) - F(V_2) \right] = \Delta V^2 F'(V), \tag{29}$$

and thus (28) is negative semi-definite if $F'(V) \geq 0$ for all V; all physically realistic friction laws satisfy this restriction [25]. Since $d\|\boldsymbol{\Delta}(\cdot, \cdot, t)\|^2/dt \leq 0$ for all t and initially $\|\boldsymbol{\Delta}(\cdot, \cdot, 0)\|^2 = 0$, the solution is unique ($\boldsymbol{q}_1 = \boldsymbol{q}_2$).

The above results can now be summarized in the following proposition:

Proposition 2 *The continuous problem* (8) *with boundary conditions* (13) *and fault interface conditions* (16) *and* (17) *is well-posed if* $|R| \leq 1$ *in the exterior boundary condition* (13) *and*

$$V F(V) \geq 0 \quad and \quad F'(V) \geq 0 \tag{30}$$

for all $V \in \mathbb{R}$.

3 Discrete Formulation: Stability and Energy Dissipation

We discretize the governing equations (8) using $(N_x + 1) \times (N_y + 1)$ grids on both sides of the fault with collocated grid nodes at the interface (see Fig. 1a). In the x-direction the grid indices are $i = 0, \ldots, N_x$ and in the y-direction for $y > 0$ the grid indices are $j = 0, \ldots, N_y$ and for $y < 0$ they are $j = -N_y, \ldots, 0$. A method of lines discretization using SBP operators is then

$$\frac{d\boldsymbol{q}^{(l)}}{dt} = \boldsymbol{D}_x \boldsymbol{q}^{(l)} + \boldsymbol{D}_y \boldsymbol{q}^{(l)}, \tag{31}$$

$$\boldsymbol{D}_x = \boldsymbol{H}_x^{-1} \boldsymbol{Q}_x \otimes \boldsymbol{I}_y \otimes \boldsymbol{A}_x, \qquad \boldsymbol{D}_y = \boldsymbol{I}_x \otimes \boldsymbol{H}_y^{-1} \boldsymbol{Q}_y \otimes \boldsymbol{A}_y, \tag{32}$$

$$\boldsymbol{q}^{(l)} = \begin{bmatrix} \boldsymbol{q}_0^{(l)} \\ \vdots \\ \boldsymbol{q}_{N_x}^{(l)} \end{bmatrix}, \qquad \boldsymbol{q}_i^{(1)} = \begin{bmatrix} \boldsymbol{q}_{i0}^{(1)} \\ \vdots \\ \boldsymbol{q}_{iN_y}^{(1)} \end{bmatrix}, \qquad \boldsymbol{q}_i^{(2)} = \begin{bmatrix} \boldsymbol{q}_{i,-N_y}^{(2)} \\ \vdots \\ \boldsymbol{q}_{i0}^{(2)} \end{bmatrix}, \tag{33}$$

where $q_{ij}^{(l)}$ is the grid data at grid point (ij), $H_x^{-1}Q_x$ is the 1-D SBP operator for an $(N_x + 1)$ grid, I_x is the $(N_x + 1) \times (N_x + 1)$ identity matrix (and similarly for H_y, Q_y, and I_y), and $\otimes$ is the Kronecker product of two matrices defined as

$$A \otimes B = \begin{bmatrix} A_{11}B & \cdots & A_{1N}B \\ \vdots & \ddots & \vdots \\ A_{M1}B & \cdots & A_{MN}B \end{bmatrix}. \tag{34}$$

Two Kronecker product identities are needed for the analysis that follows:

$$(A \otimes B)^T = A^T \otimes B^T \quad \text{and} \quad (A \otimes B)(C \otimes D) = (AC) \otimes (BD). \tag{35}$$

Here we only consider a homogeneous elastic medium thus allowing the use of a Kronecker product in the discretization, for heterogeneous mediums this more compact notation is not possible.

The discrete energy norm is defined in an analogous manner to the continuous energy norm (23):

$$\|q\|_h^2 = \sum_{l=1}^{2} (q^{(l)})^T (H_x \otimes H_y \otimes I_3) q^{(l)}$$

$$= \sum_{l=1}^{2} \left[\frac{\rho}{2} (v_z^{(l)})^T (H_x \otimes H_y) v_z^{(l)} + \frac{1}{2G} (\sigma_{iz}^{(l)})^T (H_x \otimes H_y) \sigma_{iz}^{(l)} \right], \tag{36}$$

where the first term is the kinetic energy, the second the elastic strain energy, and $I_3 = \text{diag}[1\ 1\ 1]$. The difference operator is said to be strictly stable [8] if

$$\|q(t)\|_h^2 \leq K_d e^{\alpha_d t} \|q(0)\|_h^2, \quad \alpha_d \leq \alpha_c + \mathcal{O}(h), \tag{37}$$

where α_d and K_d are constants independent of the initial conditions and α_c is the growth rate for the continuous problem in (22). If it can be shown that the discrete solution dissipates energy at least as fast as the continuous solution, and that the energy dissipation rate converges to the true rate under refinement, then (37) follows.

For the discrete method to be fully specified, the boundary and interface conditions must be included. In this work two methods are considered: the injection method (strong enforcement) and the SAT method (weak enforcement).

3.1 SBP + Injection Method

In the injection method, boundary conditions are enforced strongly so that the boundary values strictly satisfy the boundary conditions. This can be done by modifying the characteristic variables associated with waves propagating from the boundary or fault into the medium [11, 23, 31, 32]; we assume that the boundary and interface conditions are in characteristic form, (13) and (14). Given grid data $q_{ij}^{(l)}$, we define a new variable $\hat{q}_{ij}^{(l)}$ which in the interior of the domain ($i \neq 0, N_x$ and $j \neq 0, \pm N_y$) is the original grid data $\hat{q}_{ij}^{(l)} = q_{ij}^{(l)}$ but on the boundary and fault is modified to satisfy these conditions. For example, at the fault $\hat{q}_{i0}^{(l)}$ is defined as

$$\hat{q}_{i0}^{(l)} = \frac{1}{2\sqrt{2\rho}} \begin{bmatrix} \mathcal{W}_{i0}^{-(l)} - w_{i0}^{+(l)} \\ \mathring{w}_{i0}^{(l)} \\ n_y^{(l)}(\mathcal{W}_{i0}^{-(l)} + w_{i0}^{+(l)}) \end{bmatrix}, \tag{38}$$

$$\mathcal{W}_{i0}^{-(l)} \equiv \mathcal{W}^{-(l)} \left(w_{i0}^{+(1)}, w_{i0}^{+(2)} \right), \tag{39}$$

where $w_{ij}^{+(l)}$ is the characteristic variable propagating into the fault defined from the grid data $\boldsymbol{q}_{ij}^{(l)}$. The exterior boundary nodes are modified in an analogous manner. It is clear that in (38) only the inward propagating characteristic variable $w_{ij}^{-(l)}$ is modified and that, by construction, $\hat{\boldsymbol{q}}^{(l)}$ now strictly satisfies the boundary and interface conditions.

The injection method can now be stated as

$$\frac{d\boldsymbol{q}^{(l)}}{dt} = \boldsymbol{D}_x \hat{\boldsymbol{q}}^{(l)} + \boldsymbol{D}_y \hat{\boldsymbol{q}}^{(l)}, \tag{40}$$

with $\boldsymbol{D}_x$ and $\boldsymbol{D}_y$ given in (32). Since the injection method amounts to modifying the difference operator, the SBP property of the operator is lost and, in general, it is not possible to prove that the resulting method satisfies the stability condition (37) [8, 15]. This can lead to unbounded energy growth in the numerical solution, as will be seen in the computational results below.

3.2 SBP + SAT (Simultaneous Approximation Term) Method

In the SAT method, boundary conditions are weakly enforced through penalty terms added directly to the semi-discretized system:

$$\frac{d\boldsymbol{q}^{(1)}}{dt} = \boldsymbol{D}_x \boldsymbol{q}^{(1)} + \boldsymbol{D}_y \boldsymbol{q}^{(1)} + \boldsymbol{BT}_N^{(1)} + \boldsymbol{FT}^{(1)} + \boldsymbol{BT}_E^{(1)} + \boldsymbol{BT}_W^{(1)}, \tag{41}$$

$$\frac{d\boldsymbol{q}^{(2)}}{dt} = \boldsymbol{D}_x \boldsymbol{q}^{(2)} + \boldsymbol{D}_y \boldsymbol{q}^{(2)} + \boldsymbol{FT}^{(2)} + \boldsymbol{BT}_S^{(2)} + \boldsymbol{BT}_E^{(2)} + \boldsymbol{BT}_W^{(2)}, \tag{42}$$

$$\boldsymbol{BT}_W^{(l)} = \left(\boldsymbol{H}_x^{-1} \otimes \boldsymbol{I}_y \otimes \boldsymbol{\Sigma}_W^{(l)} \right) \left[\boldsymbol{e}_W \otimes \left(\boldsymbol{w}_W^{-(l)} - \boldsymbol{R}_W^{(l)} \boldsymbol{w}_W^{+(l)} \right) \otimes \boldsymbol{e}_3 \right], \tag{43}$$

$$\boldsymbol{FT}^{(1)} = \left(\boldsymbol{I}_x \otimes \boldsymbol{H}_y^{-1} \otimes \boldsymbol{\Sigma}^{(1)} \right) \left[\boldsymbol{B}^{(1)} \left(\boldsymbol{q}^{(1)}, \boldsymbol{q}^{(2)} \right) \otimes \boldsymbol{e}_S \otimes \boldsymbol{e}_3 \right], \tag{44}$$

$$\boldsymbol{FT}^{(2)} = \left(\boldsymbol{I}_x \otimes \boldsymbol{H}_y^{-1} \otimes \boldsymbol{\Sigma}^{(2)} \right) \left[\boldsymbol{B}^{(2)} \left(\boldsymbol{q}^{(1)}, \boldsymbol{q}^{(2)} \right) \otimes \boldsymbol{e}_N \otimes \boldsymbol{e}_3 \right]. \tag{45}$$

The other exterior boundary penalty terms are defined in a similar manner to $\boldsymbol{BT}_W^{(l)}$; $\boldsymbol{e}_3 = [1\ 1\ 1]^T$, vectors $\boldsymbol{e}_S = [1\ 0\ \cdots\ 0]^T$ and $\boldsymbol{e}_N = [0\ \ldots\ 0\ 1]$ are of size $(N_y + 1) \times 1$ (similarly for $\boldsymbol{e}_E$ and $\boldsymbol{e}_W$ except that they are of size $(N_x + 1) \times 1$). In the penalty terms $\boldsymbol{w}_W^{\pm(l)}$ is the $(N_y + 1) \times 1$ vector of characteristic variables defined from the grid data at the west boundary, that is, from the data

$$\boldsymbol{q}_W = \left(\boldsymbol{e}_W^T \otimes \boldsymbol{I}_y \right) \boldsymbol{q}. \tag{46}$$

A similar definition applies to variables $\boldsymbol{w}_{N/S/E}^{\pm(l)}$. In the exterior boundary term we define

$$\boldsymbol{R}_W^{(1)} = \mathbf{diag} \left[R_W^{(1)}(y=0) \ \cdots \ R_W^{(1)}(y=L_y) \right], \tag{47}$$

$$\boldsymbol{R}_W^{(2)} = \mathbf{diag} \left[R_W^{(2)}(y=-L_y) \ \cdots \ R_W^{(2)}(y=0) \right], \tag{48}$$

with similar definitions applying to the other reflection coefficient matrices. For the fault interface condition we consider two different formulations for the fault interface conditions,

$B^{(l)}$, based on (17) and (14), respectively. The first is the non-characteristic formulation:

$$B_{nc}^{(l)} = \begin{bmatrix} \left(\sigma_{yz}^{(l)}\right)_{00} - F\left(\left(v_z^{(1)}\right)_{00} - \left(v_z^{(2)}\right)_{00}\right) \\ \vdots \\ \left(\sigma_{yz}^{(l)}\right)_{N_x0} - F\left(\left(v_z^{(1)}\right)_{N_x0} - \left(v_z^{(2)}\right)_{N_x0}\right) \end{bmatrix} = (\sigma_{yz})_F^{(l)} - F(V), \qquad (49)$$

and the second is the characteristic formulation:

$$B_c^{(l)} = \begin{bmatrix} w_{00}^{-(l)} - \mathcal{W}_{00}^{-(l)} \\ \vdots \\ w_{N_x0}^{-(l)} - \mathcal{W}_{N_x0}^{-(l)} \end{bmatrix} = \boldsymbol{w}_F^{-(l)} - \boldsymbol{\mathcal{W}}_F^{-(l)}, \qquad (50)$$

where the subscript F refers data at the fault nodes stacked as a vector and $\boldsymbol{\mathcal{W}}_F^{-(l)}$ is the interface relation (14) evaluated at each of the fault nodes in a similar vector form. Due to the fact that there is only one boundary condition per direction at each boundary node, the penalty matrices $\boldsymbol{\Sigma}$ can be taken to be diagonal matrices, i.e., for the fault terms $\boldsymbol{\Sigma}^{(l)} = \mathbf{diag}[\Sigma_1^{(l)} \; \Sigma_2^{(l)} \; \Sigma_3^{(l)}]$ and similarly for the other penalty matrices. Note that the penalty terms are identically zero if the grid data exactly satisfies the boundary conditions or friction law.

The energy dissipation rate of the method is

$$\frac{d}{dt}\|\boldsymbol{q}(t)\|_h^2 = \sum_{l=1}^{2}\left[\frac{d(\boldsymbol{q}^{(l)})^T}{dt}\left(\boldsymbol{H}_x \otimes \boldsymbol{H}_y \otimes \boldsymbol{I}_3\right)\boldsymbol{q}^{(l)}\right.$$
$$\left. + \left(\boldsymbol{q}^{(l)}\right)^T\left(\boldsymbol{H}_x \otimes \boldsymbol{H}_y \otimes \boldsymbol{I}_3\right)\frac{d\boldsymbol{q}^{(l)}}{dt}\right]$$
$$= \sum_{l=1}^{2}\left(BT_E^{(l)} + BT_W^{(l)}\right) + BT_N^{(1)} + BT_S^{(2)} + FT^{(1)} + FT^{(2)}, \qquad (51)$$

where the west boundary term is obtained using the SBP property (6) as

$$BT_W^{(l)} = -\left(\boldsymbol{q}^{(l)}\right)^T\left(\boldsymbol{E}_W \otimes \boldsymbol{H}_y \otimes \boldsymbol{A}_x\right)\boldsymbol{q}^{(l)}$$
$$+ 2\left(\boldsymbol{q}^{(l)}\right)^T\left(\boldsymbol{E}_W \otimes \boldsymbol{H}_y \otimes \boldsymbol{\Sigma}_W^{(l)}\right)\left[\boldsymbol{e}_W \otimes \left(\boldsymbol{w}_W^{-(l)} - \boldsymbol{R}_W^{(l)}\boldsymbol{w}_W^{+(l)}\right) \otimes \boldsymbol{e}_3\right]$$
$$= -\left(\boldsymbol{v}_z^{(l)}\right)_W^T \boldsymbol{H}_y\left(\boldsymbol{\sigma}_{xz}^{(l)}\right)_W$$
$$+ 2\left(\boldsymbol{q}_W^{(l)}\right)^T\left[\boldsymbol{H}_y\left(\boldsymbol{w}_W^{-(l)} - \boldsymbol{R}_W^{(l)}\boldsymbol{w}_W^{+(l)}\right) \otimes \boldsymbol{\Sigma}_W^{(l)}\boldsymbol{e}_3\right], \qquad (52)$$

with $\boldsymbol{E}_W = \mathbf{diag}(\boldsymbol{e}_W)$. Analogous expressions exist for the other boundary terms $BT_E^{(l)}$, $BT_N^{(1)}$, and $BT_S^{(2)}$. The fault terms are

$$FT^{(1)} = -\left(\boldsymbol{v}_z^{(1)}\right)_F^T \boldsymbol{H}_x\left(\boldsymbol{\sigma}_{yz}^{(1)}\right)_F + 2\left(\boldsymbol{q}_F^{(1)}\right)^T\left(\boldsymbol{H}_x \boldsymbol{B}^{(1)} \otimes \boldsymbol{\Sigma}^{(1)}\boldsymbol{e}_3\right), \qquad (53)$$

$$FT^{(2)} = \left(\boldsymbol{v}_z^{(2)}\right)_F^T \boldsymbol{H}_x\left(\boldsymbol{\sigma}_{yz}^{(2)}\right)_F + 2\left(\boldsymbol{q}_F^{(2)}\right)^T\left(\boldsymbol{H}_x \boldsymbol{B}^{(2)} \otimes \boldsymbol{\Sigma}^{(2)}\boldsymbol{e}_3\right). \qquad (54)$$

We will now discuss the choice of the penalty matrix for the west boundary term. Replacing the physical variables with the characteristic variables in (52), we have

$$BT_W^{(l)} = -\frac{1}{4Z}\big[(\boldsymbol{w}_W^{+(l)})^T \boldsymbol{H}_y \boldsymbol{w}_W^{+(l)} - (\boldsymbol{w}_W^{-(l)})^T \boldsymbol{H}_y \boldsymbol{w}_W^{-(l)}\big]$$
$$+ 2(\boldsymbol{q}_W^{(l)})^T \big[\boldsymbol{H}_y(\boldsymbol{w}_W^{-(l)} - \boldsymbol{R}_W^{(l)} \boldsymbol{w}_W^{+(l)}) \otimes \Sigma_W^{(l)} \boldsymbol{e}_3\big]. \tag{55}$$

Making the choice of $\Sigma_W^{(l)} = -(1/2\sqrt{2\rho})\,\mathbf{diag}[1\ -1\ 0]$ such that

$$(\boldsymbol{q}^{(l)})_{ij}^T \Sigma_W^{(l)} \boldsymbol{e}_3 = -\frac{1}{4Z}(w_W^{-(l)})_{ij}, \tag{56}$$

the west boundary term becomes

$$BT_W^{(l)} = -\frac{1}{4Z}(\boldsymbol{w}_W^{+(l)})^T (\boldsymbol{H}_y - \boldsymbol{R}_W \boldsymbol{H}_y \boldsymbol{R}_W)\,\boldsymbol{w}_W^{+(l)}$$
$$-\frac{1}{4Z}(\boldsymbol{w}^{-(l)} - \boldsymbol{R}_W^{(l)} \boldsymbol{w}_W^{+(l)})^T \boldsymbol{H}_y(\boldsymbol{w}^{-(l)} - \boldsymbol{R}_W^{(l)} \boldsymbol{w}_W^{+(l)}). \tag{57}$$

This is negative semi-definite if $\boldsymbol{H}_y - \boldsymbol{R}_W \boldsymbol{H}_y \boldsymbol{R}_W$ is positive semi-definite. For the diagonal norm (i.e., when $\boldsymbol{H}_y$ is a diagonal matrix), which we exclusively use in this paper, there are no new restrictions on the reflection coefficients.

Thus, all the exterior boundary terms are negative semi-definite, dissipating energy slightly faster than the continuous problem (26) and leading to a strictly stable scheme if the penalty matrices for the fault terms can be appropriately chosen as well.

Remark If the block norm operators are used, then the requirement that $\boldsymbol{H}_y - \boldsymbol{R}_W \boldsymbol{H}_y \boldsymbol{R}_W$ is positive semi-definite places restrictions on the spatial variability of the reflection coefficients near grid corners. This restriction on $\boldsymbol{R}$ is independent of the choice of the penalty matrix since if in (55) the grid data satisfies the boundary condition exactly, i.e., $\boldsymbol{w}_W^{-(l)} = \boldsymbol{R}_W^{(l)} \boldsymbol{w}_W^{+(l)}$, then

$$BT_W^{(l)} = -\frac{1}{4Z}(\boldsymbol{w}_W^{+(l)})^T (\boldsymbol{H}_y - \boldsymbol{R}_W^{(l)} \boldsymbol{H}_y \boldsymbol{R}_W^{(l)})\boldsymbol{w}_W^{+(l)}, \tag{58}$$

regardless of the choice of the penalty matrix $\Sigma_W^{(l)}$.

3.2.1 Non-characteristic Fault Treatment

Summing (53) and (54) and dropping the subscript F, i.e., all grid data refers to grid data at the fault, we have

$$FT^{(1)} + FT^{(2)}$$
$$= -(\boldsymbol{v}_z^{(1)})^T \boldsymbol{H}_x \boldsymbol{\sigma}_{yz}^{(1)} + (\boldsymbol{v}_z^{(2)})^T \boldsymbol{H}_x \boldsymbol{\sigma}_{yz}^{(2)}$$
$$+ 2\sum_{l=1}^{2}\left(\sqrt{\frac{\rho}{2}}\boldsymbol{v}_z^{(l)}\Sigma_1^{(l)} + \frac{\boldsymbol{\sigma}_{xz}^{(l)}}{\sqrt{2G}}\Sigma_2^{(l)} + \frac{\boldsymbol{\sigma}_{yz}^{(l)}}{\sqrt{2G}}\Sigma_3^{(l)}\right)^T \boldsymbol{H}_x\big(\boldsymbol{\sigma}_{yz}^{(l)} - \boldsymbol{F}(V)\big). \tag{59}$$

Picking $\Sigma_1^{(1)} = -\Sigma_1^{(2)} = 1/\sqrt{2\rho}$ and $\Sigma_2^{(l)} = \Sigma_3^{(l)} = 0$ this becomes

$$FT^{(1)} + FT^{(2)} = -V^T H_x F(V), \tag{60}$$

which, if $V^T H_x F(V) \geq 0$, is nonpositive. For diagonal H_x this requirement is satisfied if $V F(V) \geq 0$ at every point.

Interpreting the slip velocity as V and the fault strength as $\tau = F(V)$, the method dissipates energy at the same rate as the continuous problem (25) and is strictly stable (there is no additional damping with this method).

Remark If one uses the block norm SBP operators the restriction that $V^T H_x F(V) \geq 0$ needs to be verified. As is the case for the exterior boundaries, this additional requirement on the spatial variation of $F(V)$ is not a result of the choice of the penalty matrices.

In a completely analogous manner to the continuous problem, we can summarize the results for the non-characteristic fault treatment in the following proposition:

Proposition 3 *The semi-discrete problem* (41) *with non-characteristic fault treatment* (49) *is strictly stable if* $V^T H_x F(V) \geq 0$ *for all* V.

3.2.2 Characteristic Fault Treatment

A similar calculation can be performed for the characteristic boundary formulation (50) and the energy dissipation rate at the fault is

$$
\begin{aligned}
FT^{(1)} + FT^{(2)} \\
= \sum_{l=1}^{2} \Bigg[\frac{1}{4Z} \big(w^{-(l)} - w^{+(l)}\big)^T H_x \big(w^{-(l)} + w^{+(l)}\big) \\
+ 2 \left(\sqrt{\frac{\rho}{2}} v_z^{(l)} \Sigma_1^{(l)} + \frac{\sigma_{xz}^{(l)}}{\sqrt{2G}} \Sigma_2^{(l)} + \frac{\sigma_{yz}^{(l)}}{\sqrt{2G}} \Sigma_3^{(l)} \right)^T H_x \big(w^{-(l)} - \mathcal{W}^{-(l)}\big) \Bigg].
\end{aligned} \tag{61}
$$

Picking $\Sigma_1^{(l)} = -\Sigma_3^{(1)} = \Sigma_3^{(2)} = -1/(2\sqrt{2\rho})$ and $\Sigma_2^{(l)} = 0$, this becomes

$$
\begin{aligned}
FT^{(1)} + FT^{(2)} &= -\frac{1}{4Z} \sum_{l=1}^{2} \big[\big(w^{+(l)}\big)^T H_x w^{+(l)} - \big(\mathcal{W}^{-(l)}\big)^T H_x \mathcal{W}^{-(l)} \\
&\quad + \big(w^{-(l)} - \mathcal{W}^{-(l)}\big)^T H_x \big(w^{-(l)} - \mathcal{W}^{-(l)}\big) \big] \\
&= -\frac{1}{4Z} \sum_{l=1}^{2} \big[\big(w^{+(l)} - \mathcal{W}^{-(l)}\big)^T H_x \big(w^{+(l)} + \mathcal{W}^{-(l)}\big) \\
&\quad + \big(w^{-(l)} - \mathcal{W}^{-(l)}\big)^T H_x \big(w^{-(l)} - \mathcal{W}^{-(l)}\big) \big].
\end{aligned} \tag{62}
$$

Defining

$$\hat{v}_z^{(l)} = \frac{1}{2Z} \big(w^{+(l)} - \mathcal{W}^{-(l)}\big), \qquad \hat{V} = \hat{v}_z^{(1)} - \hat{v}_z^{(2)}, \tag{63}$$

$$\hat{\boldsymbol{\sigma}}_{yz}^{(1)} = -\frac{1}{2}\left(\boldsymbol{w}^{+(1)} + \boldsymbol{\mathcal{W}}^{-(1)}\right), \qquad \hat{\boldsymbol{\sigma}}_{yz}^{(2)} = \frac{1}{2}\left(\boldsymbol{w}^{+(2)} + \boldsymbol{\mathcal{W}}^{-(2)}\right), \tag{64}$$

we have that $\hat{\boldsymbol{\tau}} = \hat{\boldsymbol{\sigma}}_{yz}^{(l)} = \boldsymbol{F}(\hat{V})$ due to the fact that $\mathcal{W}^{-(l)}$ is derived from the friction law (17) and continuity of traction components of stress (16); see (18) and (19). Using these definitions in (62) gives

$$FT^{(1)} + FT^{(2)} = -\hat{\boldsymbol{V}}^T \boldsymbol{H}_x \boldsymbol{F}(\hat{V}) - \frac{1}{4Z}\sum_{l=1}^{2}\left(\boldsymbol{w}^{+(l)} - \boldsymbol{\mathcal{W}}^{-(l)}\right)^T \boldsymbol{H}_x\left(\boldsymbol{w}^{+(l)} - \boldsymbol{\mathcal{W}}^{-(l)}\right). \tag{65}$$

If $\hat{\boldsymbol{V}}^T \boldsymbol{H}_x \boldsymbol{F}(\hat{V}) \geq 0$ (the same requirement as was needed for the non-characteristic boundary treatment), the method dissipates energy at the same rate as the continuous problem (25) plus a small numerical damping term and is strictly stable.

We thus have the following proposition:

Proposition 4 *The semi-discrete problem* (41) *with characteristic fault treatment* (50) *is strictly stable if* $\hat{\boldsymbol{V}}^T \boldsymbol{H}_x \boldsymbol{F}(\hat{V}) \geq 0$ *for all* $\hat{V}$.

In the Appendix we discuss the implementation and interpretation of the difference method with characteristic fault treatment and diagonal norm operators.

3.3 Reduction of the Method to 1-D

Here we briefly present how the above methods can be reduced to 1-D. We do this because it is easier to analyze the computational efficiency differences between the characteristic and non-characteristic SAT methods for the 1-D equations. Additionally, the effect of the lack of strict stability for the injection method is easily seen for the 1-D problem where analytic solutions are easily derived and time-scales over which instabilities will be manifest can be computed. The difference operator (31) is reduced to 1-D by setting $\boldsymbol{D}_x = 0$ and $\boldsymbol{I}_x = 1$. Similarly, the injection method still takes the form of (40) with $\hat{\boldsymbol{q}} = \boldsymbol{q}$ except at the fault, north, and south boundaries where it is defined by (38).

For the SAT method (41), $\boldsymbol{BT}_W^{(l)} = \boldsymbol{BT}_E^{(l)} = \boldsymbol{0}$ and the other exterior boundary and fault terms become

$$\boldsymbol{BT}_N^{(1)} = \left(\boldsymbol{H}_y^{-1} \otimes \boldsymbol{\Sigma}_N^{(1)}\right)(\boldsymbol{e}_S \otimes \boldsymbol{e}_3)\left(\boldsymbol{w}_N^{-(1)} - R_N \boldsymbol{w}_N^{+(1)}\right), \tag{66}$$

$$\boldsymbol{BT}_S^{(2)} = \left(\boldsymbol{H}_y^{-1} \otimes \boldsymbol{\Sigma}_S^{(2)}\right)(\boldsymbol{e}_N \otimes \boldsymbol{e}_3)\left(\boldsymbol{w}_S^{-(2)} - R_S \boldsymbol{w}_S^{+(2)}\right), \tag{67}$$

$$\boldsymbol{FT}^{(1)} = \left(\boldsymbol{H}_y^{-1} \otimes \boldsymbol{\Sigma}^{(1)}\right)(\boldsymbol{e}_S \otimes \boldsymbol{e}_3)\, B^{(1)}\left(\boldsymbol{q}^{(1)}, \boldsymbol{q}^{(2)}\right), \tag{68}$$

$$\boldsymbol{FT}^{(2)} = \left(\boldsymbol{H}_y^{-1} \otimes \boldsymbol{\Sigma}^{(2)}\right)(\boldsymbol{e}_N \otimes \boldsymbol{e}_3)\, B^{(2)}\left(\boldsymbol{q}^{(1)}, \boldsymbol{q}^{(2)}\right). \tag{69}$$

Since these 1-D methods are a subset of the previously presented 2-D methods, all of the previously derived well-posedness and stability properties apply and the method is strictly stable with the given penalty matrices.

4 Stiffness and Efficiency

Two different SAT formulations have been presented; here we look at the computational advantages and disadvantages of each. The first difference is the nature of the boundary term.
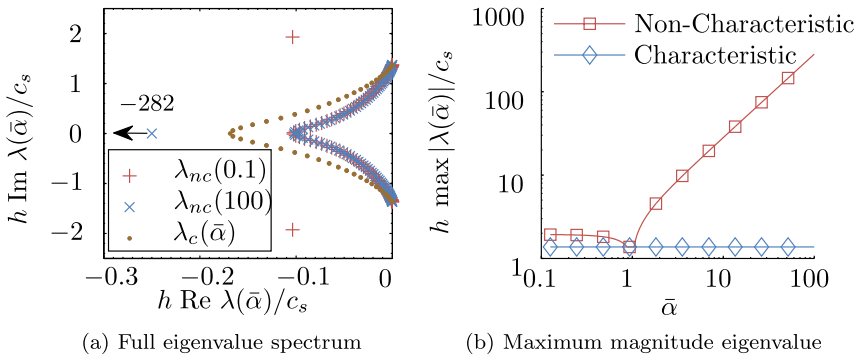
(a) Full eigenvalue spectrum   (b) Maximum magnitude eigenvalue

Fig. 3 Eigenvalues for the non-characteristic (nc) and characteristic (c) boundary treatments with the linear friction law (70). For these plots, we use $N_y = 50$ and the fourth order diagonal norm SBP operator; the overall trends are independent of N_y and the order of the operator. The spectrum $\lambda_c(\bar{\alpha})$ is largely independent of $\bar{\alpha}$, and for all values of $\bar{\alpha}$ the plot is visually the same. The purely real eigenvalue of $\lambda_{nc}(100)$ is shifted to the location indicated by the arrow and value

For the non-characteristic formulation the only computational expense associated with forming the boundary term (49) is the cost of evaluating the friction law, $F(V)$. On the other hand, the characteristic boundary formulation (50) requires solving a nonlinear system in order to calculate $\mathcal{W}^-(w^{+(1)}, w^{+(2)})$, at least when $\mathcal{W}^-$ is not expressible in closed form, which involves several evaluations of the friction law. In (18)–(20) the interface conditions $\mathcal{W}^{-(1)}$ and $\mathcal{W}^{-(2)}$ are defined implicitly and can be efficiently found with a bracketed Newton's method. In our experience, the net computational cost of the method is dominated by the difference approximation in the interior and the nonlinear solve is negligible in comparison.

A more important concern is related to the stiffness of the ODE system, which influences the maximum time step that can be used with explicit time integration methods. To understand this, we consider the methods in 1-D. Using the linear friction law

$$F(V) = \alpha \, V \quad \Rightarrow \quad \mathcal{W}^-(w^+) = \frac{\alpha/Z - 1}{\alpha/Z + 1} w^+ \tag{70}$$

in the two SAT formulations, with a non-reflecting exterior boundary conditions ($R = 0$), the semi-discretization is a linear system in q. From (70) we see that the friction law has introduced a single nondimensional parameter $\bar{\alpha} = \alpha/Z$. Let $\lambda_{nc}(\bar{\alpha})$ and $\lambda_c(\bar{\alpha})$ be the eigenvalue spectra for the non-characteristic and characteristic schemes, respectively, which are functions of $\bar{\alpha}$. In Fig. 3a we show $\lambda_{nc}(0.1)$, $\lambda_{nc}(100)$, and $\lambda_c(\bar{\alpha})$ (for $\lambda_c(\bar{\alpha})$ the spectrum is virtually the same for all $\bar{\alpha}$). For both formulations the whole spectrum satisfies $\text{Re}\,\lambda \leq 0$ (a consequence of strict stability) and for large $\bar{\alpha}$ the non-characteristic formulation has a large magnitude, purely real, negative eigenvalue which leads to stiffness. We can characterize stiffness by considering the maximum magnitude eigenvalue of each spectrum, shown in Fig. 3b. Stiffness increases roughly linearly with $\bar{\alpha}$ (for $\bar{\alpha} > 1$) for the non-characteristic formulation and is roughly constant for the characteristic formulation; the dip in the plot for the non-characteristic formulation is associated with a decrease in magnitude of the two "isolated" eigenvalues (seen in the spectrum of $\lambda_{nc}(0.1)$ in Fig. 3a) and the increase is associated with the increase in magnitude of the single purely real, negative eigenvalue (seen in spectrum of $\lambda_{nc}(100)$ in Fig. 3a).

The implication of this for nonlinear friction laws can be seen by linearizing a nonlinear friction law, $F(V)$, around a value V^*,

$$F(V) \approx F(V^*) + (V - V^*)\, F'(V^*), \tag{71}$$

which leads to an effective value of $\bar{\alpha} = F'(V^*)/Z$. During a single rupture simulation it is possible for the effective $\bar{\alpha}$ to range from 10^{-5} to 10^{40}. Thus, since the effective value of $\bar{\alpha}$ can be quite large or small, the non-characteristic formulation can be arbitrarily stiff, preventing efficient solution using explicit time-stepping routines. In other words, for wave propagation problems one would like $\Delta t \sim h/c_s$, that is, a time step restriction that depends predominantly on the wave propagation properties of the method and not the boundary treatment. Since the spectral radius of the non-characteristic fault treatment is unbounded, efficient explicit time integration is not possible with this formulation. For the characteristic formulation the spectral radius is bounded (and of order one) and thus it is possible to use $\Delta t \sim h/c_s$. The benefits of the characteristic formulation significantly outweigh the drawbacks and, for this reason, the rest of this work exclusively uses characteristic fault treatment.

Remark If the friction law is invertible, one could imagine instead using the boundary condition $F^{-1}(\tau) = V$ in the non-characteristic formulation. In this case, the maximum magnitude real eigenvalue of the difference operator scales roughly linearly with $1/\bar{\alpha}$ where $\bar{\alpha} = F'(V^*)/Z$ as in (71); hence, stiffness again results but now for small, instead of large, $\bar{\alpha}$.

5 Computational Results

We begin by testing the method with the previously mentioned 1-D problem configuration before proceeding to the 2-D test problem. In all of the tests the nonlinear friction law is of the form

$$F(V) = \beta \arcsinh(\gamma\, V), \tag{72}$$

where $\beta > 0$ and $\gamma > 0$; thus $F(V)$ satisfies the previously required assumptions for well-posedness. This particular functional form is widely used in earthquake mechanics and other frictional sliding problems, and has a sound theoretical basis related to how sliding is accommodated by thermally activated defect motion at microscopic contacts bridging the frictional interface [25].

Before proceeding to the results, we first present the nondimensionalization for the problems. All of the tests will have some fundamental wavenumber $k = 2\pi/\lambda$ (where λ is the fundamental wavelength) which must be resolved; this along with the wave speed c_s gives the nondimensionalized space and time variables

$$\bar{y} = ky, \quad \bar{x} = kx, \quad \bar{t} = kc_s t. \tag{73}$$

Similarly, the domain sizes can be nondimensionalized as $\bar{L}_x = kL_x$ and $\bar{L}_y = kL_y$, and in all our tests $\bar{L}_y = 50$ (and in 2-D $\bar{L}_x = \bar{L}_y$), i.e., the domain is $50\lambda/2\pi$. From the friction law (72) we note that β has units of stress, and thus we nondimensionalize stress and velocity as

$$\bar{\sigma}_{iz} = \frac{\sigma_{iz}}{\beta}, \quad \bar{v}_z = \frac{Zv_z}{\beta}. \tag{74}$$

The governing equations become

$$\frac{\partial \bar{q}}{\partial \bar{t}} = \begin{bmatrix} 0 & 1 & 0 \\ 1 & 0 & 0 \\ 0 & 0 & 0 \end{bmatrix} \frac{\partial \bar{q}}{\partial \bar{x}} + \begin{bmatrix} 0 & 0 & 1 \\ 0 & 0 & 0 \\ 1 & 0 & 0 \end{bmatrix} \frac{\partial \bar{q}}{\partial \bar{y}}, \tag{75}$$

and the friction law (72) becomes

$$\bar{F}(\bar{V}) = \operatorname{arcsinh}\left(\frac{\gamma \beta}{Z} \bar{V}\right), \tag{76}$$

where $\gamma \beta / Z$ is a single nondimensional parameter governing the behavior of the solution. In all of the 1-D tests presented here $\gamma \beta / Z = 10^4$. For the 2-D test $\gamma \beta / Z$ ranges between 10^7 and 10^{20}, which is typical for earthquake rupture simulations.

For all the test problems, error is measured with the nondimensional energy norm

$$\text{error}(N_y) = \|\bar{q}(\cdot, t_{end}) - \bar{q}(t_{end})\|_{\bar{h}}, \tag{77}$$

where $\bar{h} = kh$. The convergence rate is estimated using

$$\text{p}(N_y) = \log\left(\frac{\text{error}(N_y)}{\text{error}(2\,N_y)}\right) \bigg/ \log\left(\frac{\bar{h}(N_y)}{\bar{h}(2\,N_y)}\right), \tag{78}$$

where $\bar{h}(N_y) = \bar{L}_y / N_y$. Note that $2\pi \bar{h}^{-1}$ is the number of grid points per wavelength λ.

## 5.1 1-D Test Problems: Accuracy and the Importance of Strict Stability

For both of the 1-D test problems, the initial condition is

$$\bar{\sigma}_{yz}(\pm \bar{y}, 0) = \mp \bar{v}_z(\pm \bar{y}, 0) = 10 \, \sin(\bar{y}) \, \exp\left(-128\left(\frac{\bar{y}}{\bar{L}_y} - \frac{1}{2}\right)^2\right), \tag{79}$$

and since $\bar{\sigma}_{xz}$ is constant for this 1-D problem we do not include it in the calculation. This initial condition corresponds to a wave packet moving into the fault. We test the 2nd, 3rd, and 4th order accurate diagonal norm SBP operators (as determined by Strand [28]), where the accuracy refers to their global accuracy and the interior accuracy of the methods is 2, 4, and 6, respectively. Time integration is performed with a 4th order, low memory Runge-Kutta method of Carpenter and Kennedy [4] (5[4] method with solution 3) using a time step $\Delta \bar{t} = 0.8 \bar{h}$.

For this first test, time is truncated at $\bar{t}_{end} = \bar{L}_y$ such that the wave packet propagates into the fault and is reflected once. The exterior boundary condition is non-reflecting ($R = 0$). Figure 4 shows the results of this test; for the 1-D problems the exact solution can be constructed using the method of characteristics. Both the injection and SAT methods perform well for this test. The fact that the injection method does well suggests that the integration time is too short for erroneous energy growth, if it exists, to affect the solution. Note that the injection method is being used to enforce both the fault interface and outer boundary conditions.

The energy and error growth in the solution with time can be explored by replacing the non-reflecting boundary condition with a traction-free surface ($\sigma_{yz} = 0$ or $R = -1$) and integrating the solution until time $\bar{t}_{end} = 801 \bar{L}_y$. The wave packet interacts with the fault on
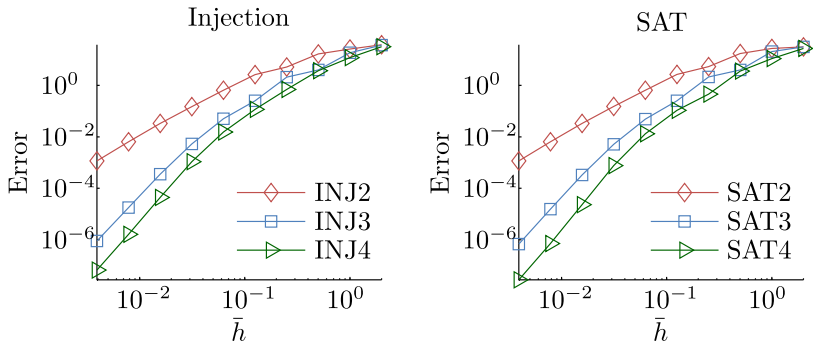
Rate Estimate:		Injection Method			SAT Method		
N_y	$\bar{h}$	2nd	3rd	4th	2nd	3rd	4th
50	1	0.6	1.0	1.4	0.2	0.6	1.3
100	2^{-1}	0.6	2.2	1.7	0.7	2.4	1.6
200	2^{-2}	1.7	0.9	2.4	1.7	0.9	3.0
400	2^{-3}	1.0	3.0	2.6	1.0	3.1	2.1
800	2^{-4}	2.0	2.3	2.9	2.0	2.4	3.0
1600	2^{-5}	2.1	3.2	3.8	2.1	3.2	4.1
3200	2^{-6}	2.2	3.9	4.6	2.2	4.0	5.0
6400	2^{-7}	2.4	4.3	4.8	2.4	4.4	5.0
12800	2^{-8}	2.5	4.3	4.6	2.5	4.5	4.7

Fig. 4 Error and convergence rate estimates for the injection and SAT methods for short time integration

the left and is reflected by the right boundary 400 times (one time for each boundary). Note that $\bar{t}/\bar{L}_y$ is the number of times that the pulse has interacted with a boundary (either the fault or the exterior boundary). Similar boundary interactions over long times are likely to arise in practical calculations involving multiple faults, Earth's surface, and other topographic features such as sedimentary basins. This test is performed for the 3rd and 4th order SBP operators with $N_y = 800$, i.e., $\bar{h}_y = 0.0625$ or 32π grid points per wavelength λ. Figure 5 shows the error (see (77)) and energy (see (36)) versus time for the methods, as well as $\bar{v}_z(y, t)$ solution profiles at select times for the 4th order methods. These plots clearly show that the energy and error grow for the injection method, whereas for the SAT method the error is bounded and energy decays at a slightly faster rate than in the exact solution, as expected.

To understand the energy growth we consider eigenvalues of the Jacobian of the injection method. We linearize the nonlinear friction law to the form (70), with effective values of $\bar{\alpha}$ calculated as in (71). For the test problem, $\bar{\alpha}$ varies between 10^{-1} and 10^4. In Fig. 6a we show the eigenvalue spectrum for both the 4th order SAT and injection methods with $\bar{\alpha} = 10$. The real portion of the spectrum is mostly negative with a large number of almost purely imaginary eigenvalues. In order to investigate the instability seen in the simulation results, Fig. 6b shows the maximum real part of the spectrum as a function of $\bar{\alpha}$ for both the 3rd and 4th order injection methods. As this plot clearly shows there is a portion of the spectrum that has a small positive real part, which is leading to the time growth in the solution energy
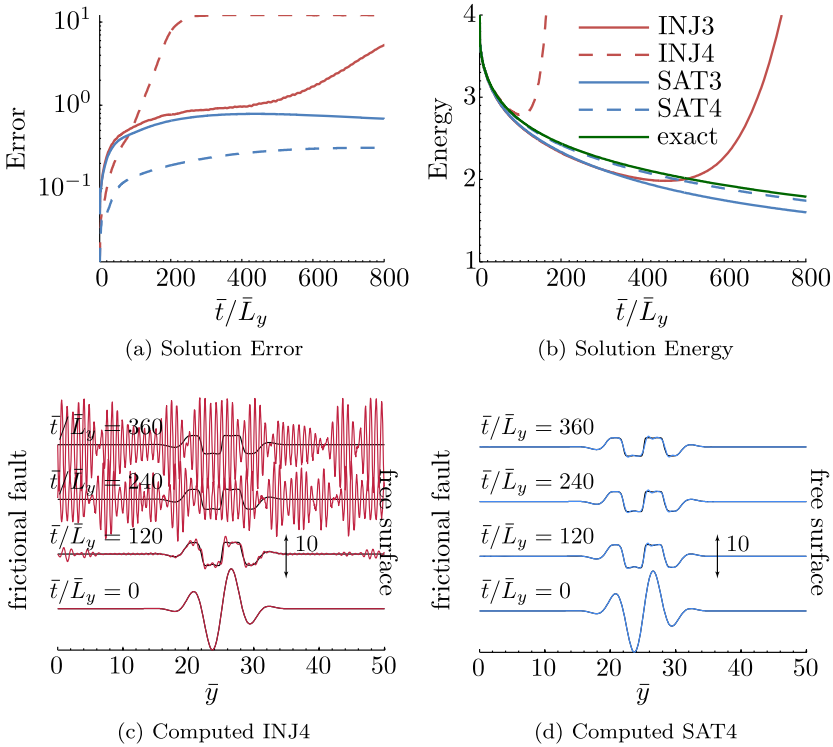
Fig. 5 (Color online) Comparison of long time integration using the injection and SAT methods. Shown are the error (**a**), energy (**b**), and $\bar{v}_z(y,t)$ at several times (**c**)–(**d**). INJ3 and INJ4 refer to the 3rd and 4th order injection methods and SAT3 and SAT4 the 3rd and 4th order SAT methods. In (**c**) and (**d**) the *black dashed line* is the exact solution and the *solid red* and *blue lines* are the computed solutions for the injection and SAT methods, respectively, at the given time

and error. A similar plot for the SAT method would show a purely negative real eigenvalue spectrum, as guaranteed by strict stability of the method.

From this analysis, the spurious energy growth in the solution occurs over a time interval

$$\frac{\bar{t}_g}{\bar{L}_y} \sim \frac{\bar{h}_y}{\bar{L}_y^2 \max \mathrm{Re}\, \lambda\,(\bar{\alpha})\,/\,k\,c_s} = \frac{1}{N_y \bar{L}_y \max \mathrm{Re}\, \lambda\,(\bar{\alpha})\,/\,k\,c_s}, \qquad (80)$$

which, from inspection of Fig. 6b, gives $\bar{t}_g/\bar{L}_y \sim 50$ for the 4th order injection method and $\bar{t}_g/\bar{L}_y \sim 250$ for the 3rd order method. These estimates are comparable with the instability times seen in Fig. 5b.

5.2 2-D Test Problem: Accuracy and Convergence

As a final test we consider a 2-D problem with the 4th order SAT method. First, note that if the material is prestressed, meaning that there are nonzero background particle velocities and stresses, then governing equations (8) can be used to model perturbations propagating on top of these background values. In this test, for $y > 0$ the background velocity is $\bar{v}_z^{(1)} = \bar{v}_0$ and for $y < 0$ the background velocity is $\bar{v}_z^{(2)} = -\bar{v}_0$; hence, there is an initial slip velocity of
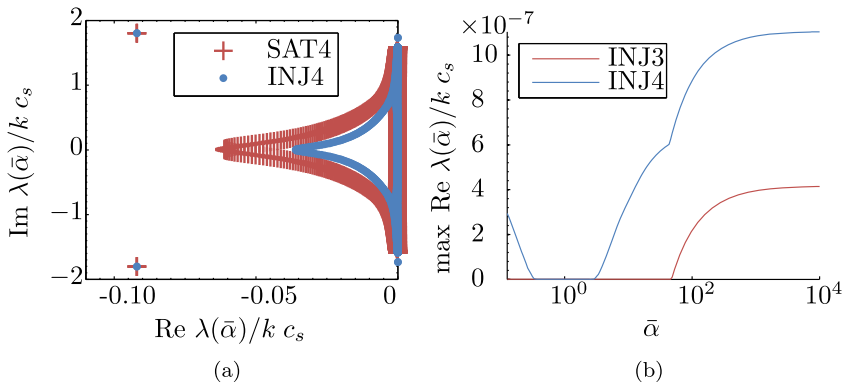
Fig. 6 (**a**) Comparison of the eigenvalue spectrum for the 4th order SAT and injection methods with a linear friction law ($\bar{\alpha} = 10$) and a traction free exterior boundary. The spectrum has a large number of almost purely imaginary eigenvalues (compare with Fig. 3a for a non-reflecting boundary condition). (**b**) The maximum real portion of the spectrum of the injection method. The existence of positive real eigenvalues explains the instability seen with long time integration (for SAT the real portion of the spectrum is strictly negative). For both plots $N_y = 800$
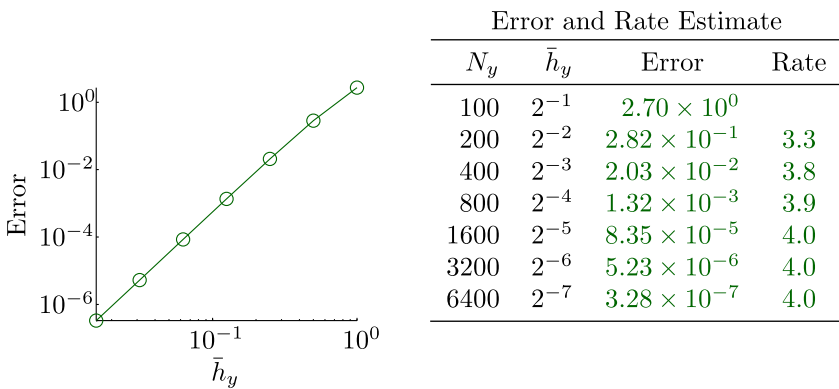

| | | Error and Rate Estimate | |
N_y	$\bar{h}_y$	Error	Rate
100	2^{-1}	2.70×10^{0}	
200	2^{-2}	2.82×10^{-1}	3.3
400	2^{-3}	2.03×10^{-2}	3.8
800	2^{-4}	1.32×10^{-3}	3.9
1600	2^{-5}	8.35×10^{-5}	4.0
3200	2^{-6}	5.23×10^{-6}	4.0
6400	2^{-7}	3.28×10^{-7}	4.0

Fig. 7 Error and convergence rate estimates for the 2-D test problems with $\bar{L}_x = \bar{L}_y = 50$ using the 4th order SAT method

$\bar{V} = \bar{v}_z^{(1)} - \bar{v}_z^{(2)} = 2\bar{v}_0$. We take $\bar{v}_0 = Z v_0 / \beta = 1$. The background stress values are $\bar{\sigma}_{xz}^{(l)} = 0$ and $\bar{\sigma}_{yz}^{(l)} = \bar{\sigma}_0 = 20$ where the friction law is defined in (76). With these background values if the initial data is identically zero, then the problem stays in steady state with the fault sliding continuously with the slip velocity $\bar{V} = 2$.

In 2-D the construction of exact solutions to general problems is more difficult, and thus we use the method of manufactured solutions (MMS) to test the method [26]. In MMS boundary data (forcing functions) and source terms are added to the problem in such a way that the exact solution is known a priori. In our case, we let the exact solution be

$$\bar{u}_z^{(1)} = -\bar{u}_z^{(2)} = (\bar{v}_0 - \varepsilon/2) J_0(\bar{r}) \sin(\bar{t}) + \bar{v}_0 \bar{t} + \bar{\sigma}_0 \bar{y}, \quad \bar{r} = \sqrt{\bar{x}^2 + \bar{y}^2}, \tag{81}$$

$$\bar{v}_z^{(l)} = \frac{\partial \bar{u}_z^{(l)}}{\partial \bar{t}}, \quad \bar{\sigma}_{xz} = \frac{\partial \bar{u}_z^{(l)}}{\partial \bar{x}}, \quad \bar{\sigma}_{yz} = \frac{\partial \bar{u}_z^{(l)}}{\partial \bar{y}}, \tag{82}$$

where $\bar{u}_z^{(l)}$ is the nondimensional displacement in the z-direction and J_0 is the Bessel function of the first kind. Displacement is measured with respect to a reference configuration in which there is no discontinuity in displacement across the fault (i.e., the initial slip is zero). The slip velocity at the origin oscillates between $\bar{V} = \varepsilon$ and $\bar{V} = 4\bar{v}_0 - \varepsilon$. We take $\varepsilon = 10^{-12}$ to render the problem highly nonlinear. With this solution, only the exterior boundary conditions and friction law need to be modified, that is, no forcing functions are needed in the interior of the domain. We do this by imposing the exact solution via a boundary condition on $\bar{v}_z$ at the exterior boundaries. The friction law (72) is modified to have $\gamma \equiv \gamma(t)$, where $\gamma(t)$ can be easily derived from (81)–(82) using $\bar{\tau}(x,t) = \bar{\sigma}_{yz}(x,0,t)$.

The exact solution (with $\bar{L}_x = \bar{L}_y = 25$) is shown in Fig. 2, and as the figure shows there are background values on top of which perturbations are propagating.

Error and convergence rate estimates are also given in Fig. 7 where a uniform grid has been used ($\bar{h}_x = \bar{h}_y = \bar{L}_y/N_y$) along with the 4th order SAT method and the simulation is run until $\bar{t}_{end} = 30$ with a time step $\bar{\Delta}t = \bar{t}_{end}/N_y = 0.3\bar{h}_y$. As these results show, after the solution is properly resolved, i.e., $\bar{h}_y = \bar{h}_x \lesssim 1$ or several grid points per wavelength, the expected rate of convergence is seen.

5.3 Energy Balance: Mechanical Energy Changes from Boundary Work and Frictional Dissipation

Of great interest to seismologists is the energy balance in earthquakes. The elastic strain energy liberated by fault slip and the accompanying relaxation of stresses in the medium is partitioned between radiated energy carried by seismic waves propagating into the far-field and energy dissipated during frictional sliding and by other inelastic processes within the fault zone [10, 27]. The radiated energy can be calculated in models like these as the work done on the material outside the domain by tractions on the exterior boundaries, provided that the boundaries are sufficiently far removed from the source. The energy dissipated in the fault zone is the work done on the fault. An appealing property of the SBP methods used in this work is the existence of a rigorously defined energy balance for the discretized problem that, as the mesh is refined, approaches the exact energy balance in the continuous problem. In this section we test two things: (1) that the numerical energy balance in the method is satisfied up to the accuracy of the scheme, and (2) that the terms in the numerical energy balance (i.e., the change in mechanical energy of the elastic body, the energy dissipated on the fault, and the work done on the body by tractions at the exterior boundaries) converge to the corresponding terms in the continuous problem.

First, we define the change in the continuous and discrete mechanical energy from (23) and (36) as

$$\Delta E(t) = \int_0^t \frac{d}{dt'} \|\boldsymbol{q}(\cdot, t')\|^2 \, dt' = \|\boldsymbol{q}(\cdot, t)\|^2 - \|\boldsymbol{q}(\cdot, 0)\|^2, \tag{83}$$

$$\Delta E_h(t) = \int_0^t \frac{d}{dt'} \|\boldsymbol{q}(t')\|_h^2 \, dt' = \|\boldsymbol{q}(t)\|_h^2 - \|\boldsymbol{q}(0)\|_h^2. \tag{84}$$

For the exact solution the change in mechanical energy is due to energy dissipation at the fault and work done at the external boundaries, which follows from (25):

$$\Delta E(t) = \int_0^t \dot{E}_b(t') \, dt' - \int_0^t \dot{E}_f(t') \, dt' = E_b(t) - E_f(t), \tag{85}$$

$$\dot{E}_b(t) = \int_{\partial\Omega} v_z \sigma_{iz} n_i \, ds, \qquad \dot{E}_f(t) = \int_{-L_x}^{L_x} V\tau \, dx, \tag{86}$$

where $\dot{E}_b$ is the energy flux through the exterior boundaries into the model domain (such that E_b is the total work done on the body) and E_f is the total energy dissipated along the fault. For the numerical solution the change in mechanical energy is of the form (85) with (86) replaced by

$$\dot{E}_{hb}(t) = \sum_{l=1}^{2} \left(BT_W^{(l)} + BT_E^{(l)} \right) + BT_N^{(1)} + BT_S^{(2)}, \tag{87}$$

$$\dot{E}_{hf}(t) = -FT^{(1)} - FT^{(2)}; \tag{88}$$

see (51). The discrete terms $\dot{E}_{hb}$ and $\dot{E}_{hf}$ differ from the continuous terms $\dot{E}_b$ and $\dot{E}_f$ in that there are grid dependent numerical dissipation terms (since we use the characteristic SAT formulation for both the fault and exterior boundaries) that go to zero as the grid is refined. Additionally, there are truncation errors associated with both the spatial discretization and time integration errors due the Runge-Kutta method.

In Fig. 8(a) we plot the terms in the energy balance for the $N_y = 3200$ numerical solution; energy is always flowing in through the exterior boundaries and being dissipated at the fault. The difference between the energy flux across the exterior boundaries and the energy dissipation rate at the fault causes the interior energy to oscillate.

The table in Fig. 8(b) shows the errors and estimated convergence rates (78) for the nondimensionalized change in mechanical energy $\Delta\bar{E}_h(\bar{t}_{end})$ and the nondimensionalized energy dissipation rate at the fault and exterior boundaries, $\dot{\bar{E}}_{hb}(\bar{t}_{end}) - \dot{\bar{E}}_{hf}(\bar{t}_{end})$, at time $\bar{t}_{end}$. Due to the absence of a pointwise error estimate (for hyperbolic equations) we cannot theoretically state how fast these terms should approach the exact values, but computationally they are seen to do so at slightly higher rates than the global accuracy of the scheme.

In the absence of time integration errors both sides of (85) would be equal, that is, the change in the energy in the solution would only be due to energy flowing across the exterior boundaries and being dissipated at the fault. The effect of the time integration errors can be quantified by integrating $\dot{E}_{hb}(t) - \dot{E}_{hf}$ throughout the simulation (using the same Runge-Kutta method used for the interior solution) and calculating

$$\Delta\bar{E}_{RK} = \Delta\bar{E}_h\left(\bar{t}_{end}\right) - \left[\bar{E}_{hb}\left(\bar{t}_{end}\right) - \bar{E}_{hf}\left(\bar{t}_{end}\right)\right]; \tag{89}$$

the calculated $\Delta\bar{E}_{RK}$ contains time integration errors from integrating the discrete equations (41) and from calculating $\bar{E}_{hb}(\bar{t}_{end}) - \bar{E}_{hf}(\bar{t}_{end})$. These errors and their estimated convergence rates are given in Fig. 8(b). As can be seen the error is decreasing at a rate comparable to the global estimated accuracy.

6 Conclusions

In this paper we have considered three ways of enforcing nonlinear boundary conditions in elastodynamics problems discretized with SBP difference operators: the injection method and two forms (non-characteristic and characteristic) of the SAT method. The injection method, though conceptually straightforward, leads to a method with a minor time instability that causes error and energy growth for problems with long time integration. On the
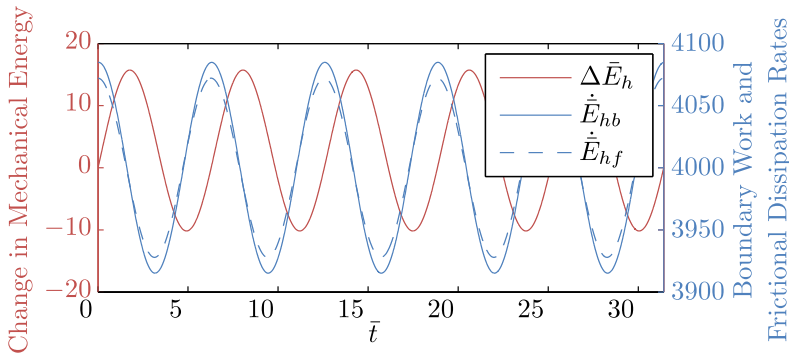
(a)

N_y	Total Energy Dissipation Rate		Total Mechanical Energy		Time Integration Error	
	Error	Rate	Error	Rate	Error	Rate
100	1.57×10^1		5.01×10^0		1.18×10^{-2}	
200	3.12×10^{-1}	5.7	1.93×10^{-1}	4.8	2.64×10^{-4}	5.6
400	4.28×10^{-3}	6.2	3.34×10^{-3}	5.9	1.50×10^{-6}	7.6
800	6.78×10^{-5}	6.0	5.93×10^{-5}	5.8	3.88×10^{-7}	2.0
1600	1.63×10^{-6}	5.4	1.34×10^{-6}	5.5	3.95×10^{-8}	3.6
3200	5.99×10^{-8}	4.8	5.10×10^{-8}	4.7	2.55×10^{-9}	4.6
6400	3.77×10^{-9}	4.0	2.79×10^{-9}	4.2	3.85×10^{-11}	6.0

(b)

Fig. 8 (a) Comparison of the change in mechanical energy $\Delta \bar{E}_h$, the energy flux across the external boundaries $\dot{\bar{E}}_{hb}$, and the rate of energy dissipation across the fault $\dot{\bar{E}}_{hf}$ versus time. (b) Error and estimated convergence rate at time $\bar{t}_{end}$ in the total mechanical energy $\Delta \bar{E}_h(\bar{t}_{end})$, the total energy dissipation rate $\dot{\bar{E}}_{hb}(\bar{t}_{end}) - \dot{\bar{E}}_{hf}(\bar{t}_{end})$, and the estimated time integration error $\Delta \bar{E}_{RK}$

other hand, both SAT methods are strictly stable, leading to numerical methods that dissipate energy at least as fast as the continuous problem (additional energy dissipation goes to zero as the mesh is refined).

The characteristic SAT method uses the boundary conditions formulated in terms of the characteristic variables in the penalty term, whereas the non-characteristic SAT method uses the boundary conditions formulated in terms of the physical variables. Though the non-characteristic method is slightly more straightforward to implement (no nonlinear solve is necessary), it leads to an arbitrarily stiff semi-discretized system, whereas the characteristic method does not. The nonlinear solve required for the characteristic method is of minimal computational cost compared to the application of the difference methods in the interior, and therefore the ability to use explicit time integration with time steps $\Delta t \sim h/c_s$ greatly outweighs this difficulty.

Three numerical tests confirm these theoretical results. The first two 1-D tests compared the characteristic SAT method to the injection method. In the first test, involving short time integration, both methods performed at their designed order of accuracy, with comparable error levels and convergence rates. The second test, involving much longer integration times,

revealed that the injection method is not strictly stable (evidenced by unphysical energy growth), whereas the SAT method is strictly stable and dissipates energy at a slightly faster rate than the continuous problem. Finally, the 2-D method was tested using the method of manufactured solutions and it displayed the expected high-order convergence rate.

For the 2-D test we also demonstrated how the seismologically important energy balance terms could be computed using SBP operators. Although no theoretical estimates exist about the expected rates at which these terms should converge for hyperbolic equations, it was demonstrated for our test problem these terms converged at roughly the scheme's global order of accuracy. The rigorously defined energy balance of our method provides a unique tool for investigating earthquake energetics. Seismologists routinely estimate both the overall change in strain energy and the radiated seismic energy. According to the energy balance equation, the difference in these two quantities is the energy dissipated on the fault. The numerical method we have developed can be used, together with seismic observations, to place unique constraints on the frictional properties of faults and the efficiency with which earthquakes convert strain energy into radiated energy.

In future work we will generalize the characteristic SAT method to full elastodynamics (involving multidirectional deformation carried by a dilatational and two shear waves with orthogonal polarizations) and faults that are governed by rate-and-state friction laws (as opposed to purely velocity dependent friction laws). We will also consider coordinate transforms which will enable the methods to be used for problems involving nonplanar faults, free surface topography, and faults which branch at various angles.

Appendix: Implementation and Interpretation with Diagonal H

In this appendix we briefly discuss the interpretation of the developed characteristic SAT method, (41) and (50), when H is diagonal. The method at an individual grid node (ij) is

$$
\begin{aligned}
\frac{d(v_z)_{ij}}{dt} = {} & \frac{1}{\rho} \sum_{k=0}^{N_x} \left(H_x^{-1} Q_x \right)_{ik} (\sigma_{xz})_{kj} + \frac{1}{\rho} \sum_{l=0}^{N_y} \left(H_y^{-1} Q_y \right)_{jl} (\sigma_{yz})_{il} \\
& - \frac{1}{2\rho} \left[H_x^{-1} \right]_{00} \left[\left(w_W^- \right)_{ij} - \left(W_W^- \right)_{ij} \right] \delta_{i0} \\
& - \frac{1}{2\rho} \left[H_x^{-1} \right]_{N_x N_x} \left[\left(w_E^- \right)_{ij} - \left(W_E^- \right)_{ij} \right] \delta_{iN_x} \\
& - \frac{1}{2\rho} \left[H_y^{-1} \right]_{00} \left[\left(w_S^- \right)_{ij} - \left(W_S^- \right)_{ij} \right] \delta_{j0} \\
& - \frac{1}{2\rho} \left[H_y^{-1} \right]_{N_y N_y} \left[\left(w_N^- \right)_{ij} - \left(W_N^- \right)_{ij} \right] \delta_{jN_y},
\end{aligned}
\tag{90}
$$

where, for simplicity, we have dropped the notation (l) indicating side of fault, δ_{kl} is the Kronecker delta, $[A]_{kl}$ denotes the kl element of the matrix A, and W^- refers to the enforced boundary condition, i.e., if ij is on the fault then $W^- = \mathcal{W}^-$. The stresses are handled similarly with $c_s/2$ instead of $1/2\rho$ multiplying the penalty terms. In this form is it clear that the penalty terms are nonzero only for grid nodes on the boundary.

For each of the penalty terms in (90) we can add and subtract w^+ to get, for instance on the south edge,

$$\frac{1}{2}\left(w_S^- - W_S^-\right) = \frac{1}{2}\left(w_S^- + w_S^+ - w_S^+ - W_S^-\right) = Z\left(v_z - \hat{v}_z^S\right), \tag{91}$$

where $\hat{v}_z^S \equiv (W_S^- - w_S^+)/2Z$. With this procedure we can write (90) as

$$\begin{aligned}
\frac{d(v_z)_{ij}}{dt} = {}& \frac{1}{\rho}\sum_{k=0}^{N_x}\left(\boldsymbol{H}_x^{-1}\boldsymbol{Q}_x\right)_{ik}(\sigma_{xz})_{kj} + \frac{1}{\rho}\sum_{l=0}^{N_y}\left(\boldsymbol{H}_y^{-1}\boldsymbol{Q}_y\right)_{jl}(\sigma_{yz})_{il} \\
& - \frac{1}{T_W}\left[(v_z)_{ij} - \left(\hat{v}_z^W\right)_{ij}\right]\delta_{i0} - \frac{1}{T_E}\left[(v_z)_{ij} - \left(\hat{v}_z^E\right)_{ij}\right]\delta_{iN_x} \\
& - \frac{1}{T_S}\left[(v_z)_{ij} - \left(\hat{v}_z^S\right)_{ij}\right]\delta_{j0} - \frac{1}{T_N}\left[(v_z)_{ij} - \left(\hat{v}_z^N\right)_{ij}\right]\delta_{jN_y},
\end{aligned} \tag{92}$$

where $T_S = [\boldsymbol{H}_y]_{00}/c_s$ and similarly for the other T values. In this form, the penalty terms can be interpreted as inducing a relaxation of the grid value v_z toward a target value $\hat{v}_z$ over the relaxation time T. Similar expressions hold for the stresses with the same relaxation times:

$$\begin{aligned}
\frac{d(\sigma_{xz})_{ij}}{dt} = {}& G\sum_{k=0}^{N_x}\left(\boldsymbol{H}_x^{-1}\boldsymbol{Q}_x\right)_{ik}(\sigma_{xz})_{kj} \\
& - \frac{1}{T_W}\left[(\sigma_{xz})_{ij} - \left(\hat{\sigma}_{xz}^W\right)_{ij}\right]\delta_{i0} - \frac{1}{T_E}\left[(\sigma_{xz})_{ij} - \left(\hat{\sigma}_{xz}^E\right)_{ij}\right]\delta_{iN_x},
\end{aligned} \tag{93}$$

$$\begin{aligned}
\frac{d(\sigma_{yz})_{ij}}{dt} = {}& G\sum_{l=0}^{N_y}\left(\boldsymbol{H}_y^{-1}\boldsymbol{Q}_y\right)_{jl}(\sigma_{xz})_{il} \\
& - \frac{1}{T_S}\left[(\sigma_{yz})_{ij} - \left(\hat{\sigma}_{yz}^S\right)_{ij}\right]\delta_{j0} - \frac{1}{T_N}\left[(\sigma_{yz})_{ij} - \left(\hat{\sigma}_{yz}^N\right)_{ij}\right]\delta_{jN_y}.
\end{aligned} \tag{94}$$

Note that the injection method (40) emerges in the limit of vanishing relaxation time. The developed SAT method can thus be interpreted as choosing a proper relaxation time so that the scheme is strictly stable.

References

1. Appelo, D., Hagstrom, T., Kreiss, G.: Perfectly matched layers for hyperbolic systems: General formulation, well-posedness, and stability. SIAM J. Appl. Math. **67**(1), 1–23 (2006). doi:10.1137/050639107
2. Carpenter, M.H., Gottlieb, D., Abarbanel, S.: Time-stable boundary conditions for finite-difference schemes solving hyperbolic systems: Methodology and application to high-order compact schemes. J. Comput. Phys. **111**(2), 220–236 (1994). doi:10.1006/jcph.1994.1057
3. Carpenter, M.H., Nordström, J., Gottlieb, D.: A stable and conservative interface treatment of arbitrary spatial accuracy. J. Comput. Phys. **148**(2), 341–365 (1999)
4. Carpenter, M.H., Kennedy, C.A.: Fourth-order 2N-storage Runge-Kutta schemes. Technical Report NASA TM-109112, National Aeronautics and Space Administration, Langley Research Center, Hampton, VA (1994)
5. Dunham, E.M., Belanger, D., Cong, L., Kozdon, J.E.: Earthquake ruptures with strongly rate-weakening friction and off-fault plasticity: 1. Planar faults. Bull. Seism. Soc. Am. (in press). URL http://pangea.stanford.edu/~edunham/publications/Dunham_etal_flat-faults_BSSA11.pdf

6. Freund, L.B.: Dynamic Fracture Mechanics, 1st edn. Cambridge University Press, Cambridge (1998)
7. Gustafsson, B.: The convergence rate for difference approximations to mixed initial boundary value problems. Math. Comput. **29**(130), 396–406 (1975)
8. Gustafsson, B., Kreiss, H.-O., Oliger, J.: Time Dependent Problems and Difference Methods. Wiley-Interscience, New York (1996)
9. Hagstrom, T., Mar-Or, A., Givoli, D.: High-order local absorbing conditions for the wave equation: Extensions and improvements. J. Comput. Phys. **227**(6), 3322–3357 (2008). doi:10.1016/j.jcp.2007.11.040
10. Kostrov, B.V.: Seismic moment and energy of earthquakes and seismic flow of rock. Izv. Earth Phys. **1**, 23–40 (1974)
11. Kreiss, H.-O.: Initial boundary value problems for hyperbolic systems. Commun. Pure Appl. Math. **23**(3), 277–298 (1970). doi:10.1002/cpa.3160230304
12. Kreiss, H.-O., Scherer, G.: Finite element and finite difference methods for hyperbolic partial differential equations. In: Mathematical Aspects of Finite Elements in Partial Differential Equations; Proceedings of the Symposium, Madison, WI, pp. 195–212 (1974)
13. Kreiss, H.-O., Scherer, G.: On the existence of energy estimates for difference approximations for hyperbolic systems. Technical report, Dept. of Scientific Computing, Uppsala University (1977)
14. Malvern, L.E.: Introduction to the Mechanics of a Continuous Medium, 1st edn. Prentice Hall, New York (1977)
15. Mattsson, K.: Boundary procedures for summation-by-parts operators. J. Sci. Comput. **18**(1), 133–153 (2003). doi:10.1023/A:1020342429644
16. Mattsson, K., Nordström, J.: Summation by parts operators for finite difference approximations of second derivatives. J. Comput. Phys. **199**(2), 503–540 (2004). doi:10.1016/j.jcp.2004.03.001
17. Mattsson, K., Ham, F., Iaccarino, G.: Stable boundary treatment for the wave equations in second-order form. J. Sci. Comput. **41**(3), 366–383 (2009). doi:10.1007/s10915-009-9305-1
18. Nordström, J.: Conservative finite difference formulations, variable coefficients, energy estimates and artificial dissipation. J. Sci. Comput. **29**(3), 375–404 (2006). doi:10.1007/s10915-005-9013-4
19. Nordström, J.: Error bounded schemes for time-dependent hyperbolic problems. SIAM J. Sci. Comput. **30**(1), 46–59 (2007). doi:10.1137/060654943
20. Nordström, J., Carpenter, M.H.: High-order finite difference methods, multidimensional linear problems, and curvilinear coordinates. J. Comput. Phys. **173**(1), 149–174 (2001). doi:10.1006/jcph.2001.6864
21. Nordström, J., Gustafsson, R.: High order finite difference approximations of electromagnetic wave propagation close to material discontinuities. J. Sci. Comput. **18**, 215–234 (2003). doi:10.1023/A:1021149523112
22. Nordström, J., Forsberg, K., Adamsson, C., Eliasson, P.: Finite volume methods, unstructured meshes and strict stability for hyperbolic problems. Appl. Numer. Math. **45**(4), 453–473 (2003). doi:10.1016/S0168-9274(02)00239-8
23. Oliger, J., Sundstrom, A.: Theoretical and practical aspects of some initial boundary value problems in fluid dynamics. SIAM J. Appl. Math. **35**(3), 419–446 (1978)
24. Olsson, P.: Summation by parts, projections, and stability. II. Math. Comput. **64**(212), 1473–1493 (1995)
25. Rice, J.R., Lapusta, N., Ranjith, K.: Rate and state dependent friction and the stability of sliding between elastically deformable solids. J. Mech. Phys. Solids **49**(9), 1865–1898 (2001). doi:10.1016/S0022-5096(01)00042-4
26. Roache, P.J.: Verification and Validation in Computational Science and Engineering. Hermosa Publishers, Albuquerque (1998)
27. Rudnicki, J.W., Freund, L.B.: On energy radiation from seismic sources. Bull. Seismol. Soc. Am. **71**(3), 583–595 (1981)
28. Strand, B.: Summation by parts for finite difference approximations for d/dx. J. Comput. Phys. **110**(1), 47–67 (1994). doi:10.1006/jcph.1994.1005
29. Svärd, M., Nordström, J.: On the order of accuracy for difference approximations of initial-boundary value problems. J. Comput. Phys. **218**(1), 333–352 (2007)
30. Svärd, M., Carpenter, M.H., Nordström, J.: A stable high-order finite difference scheme for the compressible Navier-Stokes equations, far-field boundary conditions. J. Comput. Phys. **225**(1), 1020–1038 (2007). doi:10.1016/j.jcp.2007.01.023
31. Thompson, K.W.: Time dependent boundary conditions for hyperbolic systems. J. Comput. Phys. **68**(1), 1–24 (1987). doi:10.1016/0021-9991(87)90041-6
32. Thompson, K.W.: Time-dependent boundary conditions for hyperbolic systems, II. J. Comput. Phys. **89**(2), 439–461 (1990). doi:10.1016/0021-9991(90)90152-Q